Scilight

Sustainable Engineering Novit
https://www.sciltp.com/journals/sen

Review

Check for updates

The Fusion of New Materials and Smart Technologies: Redefining How We Detect Antibiotic Resistance

Ao Qin [1,†], Yuhan Shen [1,†], Chengfeng Gao [1,2,3,4], Baosheng Chen [5,*] and Guocai Li [1,2,3,4,*]

[1] Department of Microbiology, School of Basic Medical Sciences & School of Public Health, Faculty of Medicine, Yangzhou University, Yangzhou 225001, China
[2] The Key Laboratory of the Jiangsu Higher Education Institutions for Nucleic Acid & Cell Fate Regulation, Yangzhou University, Yangzhou 225009, China
[3] Department of Academic Affairs, Guangling College, Yangzhou University, Yangzhou 225009, China
[4] The Fifth People's Hospital of Huai'an/Huai'an Hospital Affiliated to Yangzhou University, Huai'an 223300, China
[5] Department of Radiology and Bioimaging, Yale University, Newhaven, CT 06520-8042, USA
* Correspondence: baosheng.chen@yale.edu (B.C.); gcli@yzu.edu.cn (G.L.)
† These authors contributed equally to this work.

How To Cite: Qin, A.; Shen, Y.; Gao, C.; et al. The Fusion of New Materials and Smart Technologies: Redefining How We Detect Antibiotic Resistance. *Sustainable Engineering Novit* **2026**, *2*(2), 4. https://doi.org/10.53941/sen.2026.100009

Received:4 January 2026
Revised: 16 May 2026
Accepted: 2 June 2026
Published: 23 June 2026

Abstract: The global spread of antimicrobial resistance (AMR) poses an urgent threat to modern public health, driven by multiple, interacting mechanisms including enzyme inactivation, target modification, efflux pump overexpression, and biofilm formation. While conventional antimicrobial susceptibility testing (AST) and molecular techniques remain the clinical standard, their practical limitations, including time-consuming procedures, reliance on culture, inability to reveal underlying mechanisms, and poor quantification of resistance levels, highlight the urgent need for innovative solutions. This review proposes a paradigm shift in drug resistance diagnostics from static, single-indicator, endpoint detection to dynamic, multi-parameter, predictive diagnostics by integrating advanced functional materials and artificial intelligence (AI). Nanomaterials, metal-organic frameworks, graphene oxide, and microfluidic platforms allow rapid, culture-free detection of resistance enzymes, genes, and biofilms with exceptional sensitivity. Meanwhile, AI architectures—including convolutional neural networks, random forests, and graph neural networks—enable precise signal quantification, multi-modal data fusion, and accurate resistance phenotype prediction. However, clinical translation remains hindered by material reproducibility, biofouling, regulatory gaps, and cost constraints. This review provides a forward-looking roadmap for developing globally deployable, intelligent AMR diagnostic systems within a "One Health" framework.

Keywords: antimicrobial resistance; resistance mechanisms; nanomaterials; functional nucleic acids; artificial intelligence; clinical translation

1. Introduction

Antibiotics possess the remarkable ability to precisely target and eliminate pathogenic microorganisms, serving as an invisible yet vital line of defense for global public health security [1]. Widespread antibiotic overuse and improper disposal have led to their pervasive presence across diverse ecosystems. Consequently, antimicrobial resistance (AMR) and multidrug-resistant (MDR) pathogens have emerged and disseminated globally, posing one of the most severe challenges to global health in the 21st century [2,3]. In particular, the emergence of nosocomial drug-resistant "ESKAPE" pathogens (*Enterococcus faecium*, *Staphylococcus aureus*, *Klebsiella pneumoniae*, *Acinetobacter baumannii*, *Pseudomonas aeruginosa*, and *Enterobacter* species) [4] has been classified by the

World Health Organization (WHO) as critical and designated as high priority targets for the development of alternative therapies [5,6]. It is estimated that without effective interventions, AMR could lead to 10 million deaths annually worldwide by 2050 [2].

These statistics, however, obscure a deeper and more intractable problem. The clinical management of AMR is not limited solely by the dwindling pipeline of new antibiotics [7]; it is profoundly constrained by the diagnostic tools available to guide antibiotic selection at the point of care. The central diagnostic challenge extends beyond determining resistance per se: it requires sufficient speed to guide initial therapy, mechanistic insight to inform rational antibiotic selection, and quantitative precision to predict treatment outcomes. Current clinical microbiology, for all its considerable strengths, falls short on each of these interrelated fronts.

The cornerstone of clinical AMR detection remains phenotypic antimicrobial susceptibility testing (AST), principally broth microdilution [8], disk diffusion [9], and automated systems such as VITEK [10] and MicroScan [11]. These methods directly measure the inhibitory effect of an antibiotic on bacterial growth, thus providing the minimum inhibitory concentration, which is the single most clinically actionable parameter for guiding antibiotic selection. They are, however, fundamentally constrained by their absolute dependence on bacterial replication. The resulting turnaround time of 16–72 h creates a dangerous therapeutic vacuum during which clinicians must prescribe antibiotics empirically, a practice that risks both inadequate treatment of the infecting pathogen and the exertion of selective pressure driving further resistance [12]. Molecular diagnostic techniques, particularly polymerase chain reaction (PCR) in its conventional [13], quantitative [14], multiplexed [15], and digital formats [16], partially address this temporal delay by detecting resistance genes within hours rather than days. However, these genotypic methods are subject to inherent limitations. They are inherently limited to targets for which primers have been designed and cannot detect novel mutations or previously uncharacterized resistance determinants [17]. More critically, the detection of a resistance gene does not equate to its functional expression within the bacterium, nor can a single-gene or even multiplexed gene panel capture the synergistic contribution of multiple co-existing mechanisms [18]. Clinical resistance frequently results from the synergistic interplay of multiple mechanisms—for example, carbapenemase production coupled with efflux pump overexpression and porin deficiency—none of which are fully captured by conventional molecular testing [19]. This fundamental genotype-phenotype discordance can lead to both overestimation of resistance, when a detected gene is not functionally expressed, and underestimation, when phenotypic resistance arises from mechanisms not interrogated by the molecular panel.

These limitations are not merely technical inconveniences; they define three specific and addressable diagnostic gaps that this review adopts as its core analytical framework. The first is the temporal gap, the delay between clinical specimen collection and an actionable susceptibility result, which forces reliance on empirical therapy and is directly responsible for preventable mortality in severe infections such as sepsis [20]. The second is the mechanistic gap, the inability to identify, quantify, and functionally characterize the specific molecular basis of resistance, a deficiency that impedes both individualized antimicrobial therapy and population-level epidemiological surveillance [21]. The third is the interpretive gap, the failure of isolated genotypic or single-time-point phenotypic data to accurately predict the quantitative resistance phenotype and its behavior under clinically relevant conditions, such as biofilm-mode growth. This interpretive failure undermines confidence in diagnostic results and contributes to both therapeutic failure and unnecessary antibiotic overuse. Collectively, these three gaps define the design specifications for the next generation of AMR diagnostics.

This review argues that closing these gaps necessitates a paradigm shift, moving decisively from static, single-parameter, endpoint assays toward dynamic, multi-parametric, and predictive diagnostic platforms [22]. The emerging solution lies in AI-integrated diagnostic platforms: integrated platforms in which functional materials serve as high-performance, real-time sensing elements that transduce molecular interactions into quantitative signals, and AI serves as the analytical engine that decodes these complex, multi-modal data streams, fuses heterogeneous information sources, and predicts the resistance phenotype in a clinically actionable form. We conclude by situating this technological convergence within the broader imperative of transitioning from reactive antimicrobial therapy to proactive, precision stewardship.

2. Mechanisms of Bacterial Antibiotic Resistance

This section provides a concise overview of the principal resistance mechanisms to establish the biological targets for emerging diagnostic technologies. A detailed analysis of these mechanisms is essential to understand how novel materials and AI are rationally designed to overcome the specific shortcomings of traditional tests.

2.1. Antibiotic-Inactivating Enzymes

The production of antibiotic-inactivating enzymes that degrade or modify antibiotics constitutes a primary mechanism of acquired bacterial resistance [23]. β-lactamases hydrolyze the amide bond of the β-lactam ring, thereby inactivating penicillins, cephalosporins, carbapenems, and monobactams [24].

To date, thousands of β-lactamases have been identified and classified into four classes (A, B, C, D) based on amino acid sequence homology according to the Ambler classification system [25] (Figure 1). Class A enzymes include extended-spectrum β-lactamases (ESBLs, such as TEM, SHV, and CTX-M types) and some carbapenemases (e.g., KPC, SME, IMI) [26,27]. The Klebsiella pneumoniae carbapenemase (KPC) is the most globally prevalent Class A carbapenemase, capable of hydrolyzing almost all β-lactam antibiotics, including carbapenems [28]. Class B enzymes, also called metallo-β-lactamases (MBLs) such as NDM, IMP, and VIM types, require zinc ions as cofactors [24]. They hydrolyze all β-lactam drugs except aztreonam and are not affected by commonly used clinical enzyme inhibitors. The New Delhi metallo-β-lactamase (NDM) has rapidly spread worldwide since its discovery, becoming one of the most feared resistance determinants in many regions [29]. Class C enzymes, known as AmpC β-lactamases, are primarily found in Enterobacteriaceae. They hydrolyze cephalosporins but generally do not hydrolyze carbapenems [30]. Class D enzymes are the oxacillinases (OXA types), which are highly diverse. Some subtypes (e.g., OXA-48, OXA-23) possess carbapenem-hydrolyzing activity and represent a significant cause of carbapenem resistance in *Acinetobacter baumannii* and Enterobacteriaceae [31].

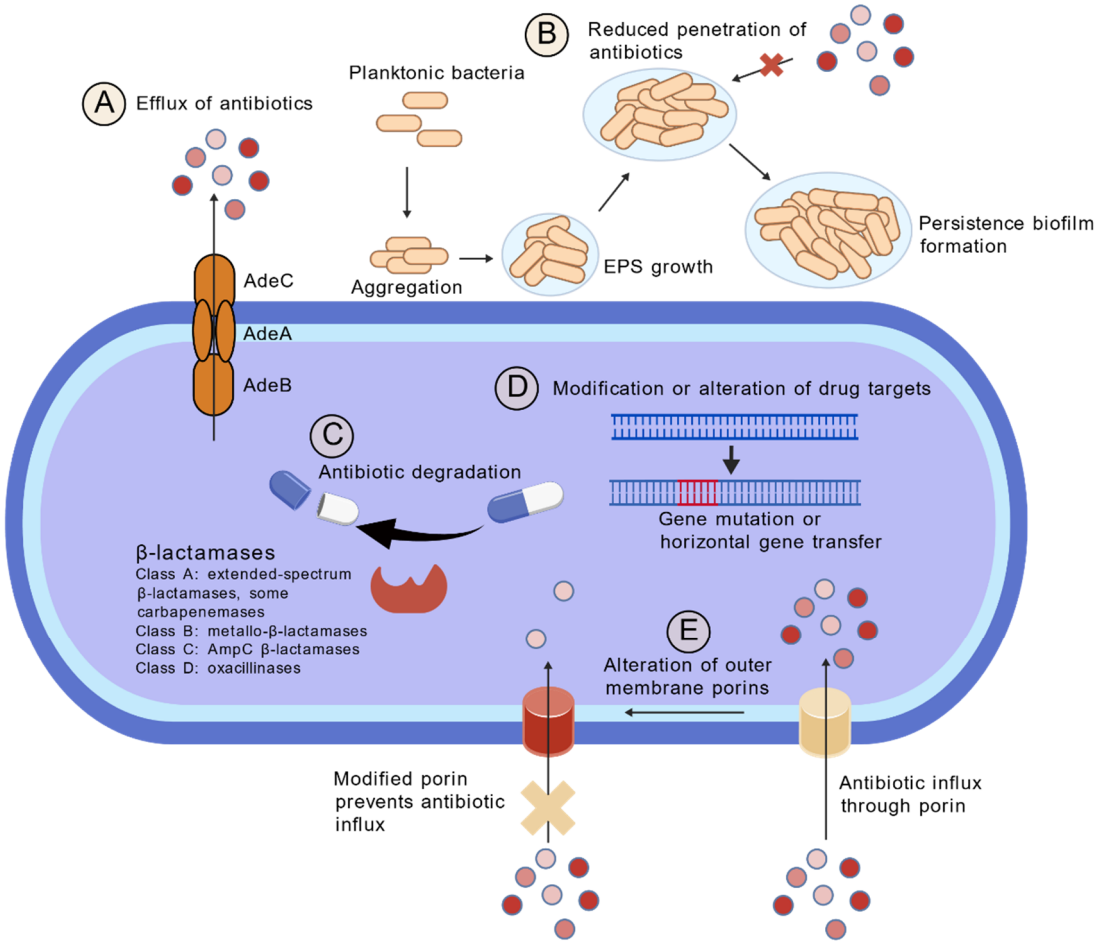

Figure 1. The Major Mechanisms of Bacterial Antimicrobial Resistance. (**A**) Increased expression of efflux pumps. (**B**) Ability to form biofilm cause high antimicrobial resistance. (**C**) β-lactamases cause enzymatic inactivation of antibiotics. (**D**) Gene mutations or horizontal gene transfer disrupt antibiotic target binding. (**E**) Reduced expression of porin or porin loss results in the decreased antibiotic entry.

Aminoglycoside-modifying enzymes (AMEs), including acetyltransferases (AACs), phosphotransferases (APHs), and nucleotidyltransferases (ANTs), covalently modify aminoglycoside antibiotics, preventing ribosomal

binding [32,33]. Differences in enzyme specificity and modification sites generate distinct resistance profiles, collectively expanding the aminoglycoside resistance spectrum [34].

These enzymes are frequently encoded on mobile genetic elements, facilitating rapid horizontal dissemination across species and genera [35]. The constant evolution of β-lactamases and AMEs, generating novel variants with altered substrate specificity from point mutations around the active site, means that detection platforms cannot rely solely on sequence-based recognition of known genes. They must functionally detect enzymatic activity to identify new variants [36].

2.2. Antibiotic Target Modification and Protection

Resistance via target modification is widespread among bacteria and arises from alterations that impede antibiotic binding to its cellular target [37]. Resistance arises when mutations occur in the genes encoding these targets, or when genes that modify the targets are acquired through horizontal gene transfer [38] (Figure 1). These changes reduce the antibiotic's affinity for its target, ultimately leading to treatment failure.

2.2.1. Target Protection

This type of target-avoidance strategy involves target protection proteins, which protect antibiotic targets from drug action [39]. One example is the ribosome protection proteins Tet(O) and Tet(M) mediate tetracycline resistance by GTP-dependent binding to the ribosome, where domain IV sterically dislodges tetracycline from its binding site without chemical modification [40,41]. Ribosome protection proteins are disseminated via plasmids and conjugative transposons and are widely distributed among different bacterial species. Furthermore, multiple related genes mediating tetracycline resistance have been identified across various hosts and must to be incorporated into resistance surveillance systems [42,43].

2.2.2. Allosteric Target Modification

FusB-family proteins employ a similar target-protection strategy by binding not to the ribosome itself but to elongation factor G (EF-G), promoting dissociation of EF-G from fusidic acid-stalled ribosome complexes and thereby conferring fusidic acid resistance [44]. Comparable allosteric target-modifying mechanisms are observed across other antibiotic classes, including tetracyclines, macrolides [45], fluoroquinolones [46], and β-lactams [47].

2.2.3. Target Site Mutation

Antibiotic resistance frequently arises from alterations in drug targets, including point mutations in target-encoding genes, enzymatic modification of binding sites, target replacement, or pathway bypass mechanisms [48].

Rifampicin resistance typically arises from single-point mutations in the rpoB gene, which encodes the β subunit of RNA polymerase. These mutations occur within the rifampicin-binding site, reducing the drug's affinity for the polymerase without significantly affecting its catalytic activity [49].

An example of resistance acquired through enzymatic modification of the binding site is ribosomal methylation catalyzed by enzymes encoded by the erm genes, which leads to macrolide resistance [50].

Vancomycin-resistant enterococci (VRE) circumvent this inhibition by acquiring van gene clusters, which modify the terminal residues to D-alanyl-D-lactate (D-Ala-D-Lac) or D-alanyl-D-serine (D-Ala-D-Ser), preventing vancomycin binding [51]. This replacement or bypass of the original target preserves peptidoglycan synthesis while rendering the bacteria resistant to the antibiotic.

These subtle molecular alterations, sometimes a single nucleotide polymorphism, demand detection methods with single-base specificity. Moreover, the co-existence of multiple target-related mechanisms within a single strain (e.g., both a target mutation and target protection) confounds single-gene PCR approaches [19]. These combined factors pose a formidable challenge to conventional diagnostic technologies.

2.3. Efflux Pumps

Efflux pumps are membrane transporters that actively extrude antibiotics and other toxic compounds, thereby lowering their intracellular concentrations (Figure 1). Although many bacteria constitutively express efflux pumps at basal levels, mutations in their encoding genes or alterations in their regulatory systems can lead to overexpression. This overexpression can confer resistance to multiple antibiotics (MDR) in bacteria [52]. Efflux pumps can be classified into five major families: the Major Facilitator Superfamily (MFS), the Small Multidrug Resistance (SMR) family, the Multidrug and Toxic Compound Extrusion (MATE) family, the Resistance-Nodulation-Division (RND) family, and the ATP-Binding Cassette (ABC) family [53]. Notable examples include

the MexAB-OprM system in *Pseudomonas aeruginosa* [54] and the AcrAB-TolC system in Enterobacteriaceae [55], both of which can expel various classes of antibiotics, contributing to bacterial multidrug resistance.

2.4. Outer Membrane Porin

The outer membrane of Gram-negative bacteria constitutes a permeability barrier that limits antibiotic influx. Many antibiotics rely on porin channels in the bacterial outer membrane to enter the cell. Mutations, deletions, or downregulation of porin-encoding genes can reduce antibiotic influx, thereby contributing to resistance (Figure 1). Hydrophilic antibiotics such as β-lactams, tetracyclines, and fluoroquinolones are particularly affected by changes in outer membrane permeability, which is especially common in carbapenem-resistant *Pseudomonas aeruginosa* [56,57] and *Acinetobacter baumannii* [58,59]. Mutations, deletions, or regulatory downregulation of porin genes, for instance *oprD* in *Pseudomonas aeruginosa*, significantly limit drug influx [60].

Clinically significant carbapenem resistance frequently arises from the synergistic combination of low-level carbapenemase activity, efflux pump upregulation, and porin deficiency. This synergy cannot be captured by genotypic tests that report only the presence or absence of a single gene, producing a critical interpretive gap [61].

2.5. Biofilms

Biofilms are structured bacterial communities embedded in a self-produced extracellular polymeric substance (EPS) matrix comprising polysaccharides, proteins, and extracellular DNA [62] (Figure 1). Biofilms confer a multi-faceted survival advantage: the matrix acts as a diffusion barrier impeding antibiotic penetration; nutrient and oxygen gradients induce slow-growing or dormant states, reducing antibiotic susceptibility by up to three orders of magnitude; and the high cell density and close proximity promote the horizontal transfer of resistance genes [63,64]. Furthermore, sub-inhibitory concentrations of antibiotics can stimulate induce biofilm formation, a clinically relevant phenomenon observed in *Acinetobacter baumannii* and *Pseudomonas aeruginosa* [65,66].

Planktonic MIC testing completely fails to predict biofilm-associated antibiotic recalcitrance. This is a profound interpretive gap, as an antibiotic declared effective by standard AST may be entirely inactive against the same pathogen growing in its biofilm state [64].

3. Traditional Antimicrobial Susceptibility Testing Methods and Their Limitations

To establish the clinical context and the rationale for technological innovation, this section reviews the current standard methods for AMR detection. We outline their operational principles and critically assess their limitations, which collectively define the diagnostic gaps that emerging material-AI platforms must address.

3.1. Antimicrobial Susceptibility Testing (AST)

Antimicrobial susceptibility testing (AST) quantifies the inhibitory effect of antibiotics on bacterial growth in vitro, providing essential data to guide clinical antimicrobial therapy [67,68]. As the standard approach in clinical microbiology laboratories, AST categorizes pathogens as susceptible, intermediate, or resistant based on established breakpoints [69]. Accurate and rapid AST is essential for guiding clinicians in the timely selection of effective antibiotics for clinical application.

Broth microdilution (BMD) is the reference for AST. It quantitatively determines the MIC by incubating a standardized bacterial inoculum with serial two-fold dilutions of an antibiotic in liquid medium, typically at 37 °C for 18–24 h for bacteria. The MIC is defined as the lowest antibiotic concentration that completely inhibits visible growth, assessed by turbidity [8,70]. BMD yields accurate, reproducible, and quantitative results. However, the method is labor-intensive, time-consuming, and susceptible to challenges including contamination, inoculum viability variability, and solvent-related inhibitory effects from compounds like dimethyl sulfoxide [71,72]. Agar dilution, conceptually similar to BMD but performed on solid medium, is particularly useful when testing a single agent against multiple isolates or when compound turbidity or coloration interferes with growth detection in broth [70,73]. It allows simultaneous testing of multiple strains on a single plate but is laborious to set up and thus less feasible for routine clinical use [74].

The disk diffusion method (Kirby-Bauer test), among the earliest established AST methods [9], involves placing paper disks containing defined amounts of antibiotics onto agar plates uniformly inoculated with the test organism. After incubation under suitable conditions, the susceptibility of the bacteria to the drug is determined by measuring the diameter of the inhibition zone formed around the disk [75]. This approach offers advantages such as simple operation, low cost, and good reproducibility. However, its results are typically qualitative (susceptible, intermediate, resistant) or semi-quantitative and do not provide a precise MIC value. Moreover,

results are highly dependent on standardized conditions, such as inoculum density, incubation time, medium composition, and the method is unreliable for slow-growing or fastidious organisms [76].

Gradient diffusion (Etest) integrates principles of both dilution and diffusion methods. A plastic strip containing a continuous, predefined antibiotic concentration gradient is placed onto an inoculated agar plate. After incubation, an ellipse-shaped inhibition zone forms, and the MIC is read directly from the scale printed on the strip at the point where the ellipse intersects the strip [77]. Etest provides a relatively simple means of obtaining an MIC value without the labor of preparing serial dilutions [78]. However, it is more costly per test than disk diffusion, and studies have indicated that for certain drug-bacterium combinations, such as vancomycin against MRSA, Etest MIC values may be systematically elevated than BMD, leading to potential misclassification [79,80].

Automated AST systems, such as VITEK [10], Trek Diagnostic Systems [81], and MicroScan WalkAway [82], have substantially improved testing throughput and standardization. These systems employ miniaturized broth dilution panels and automated readout via turbidimetry or fluorometry, reducing time to result reporting to 4–18 h [11]. However, they involve high initial capital investment and ongoing maintenance costs. The fixed antibiotic panels and concentration ranges may fail to detect certain rare or emerging resistance phenotypes. Moreover, automated systems frequently fail to detect subtle resistance phenotypes such as heterogeneous vancomycin-intermediate *S. aureus* (hVISA) [83,84].

Despite widespread use, all culture-based AST methods share a fundamental limitation: dependence on bacterial growth. This imposes a turnaround time of 16–72 h from sample receipt to result reporting [85]. In severe infections such as sepsis, mortality increases sharply with each hour of delay in administering effective therapy [12], and this temporal gap forces clinicians to rely on empirical, broad-spectrum antibiotics—a practice that increases selective pressure for resistance, risks treatment failure, and may cause unnecessary toxicity [86].

Furthermore, certain resistance mechanisms produce low levels of resistance proteins or enzymes or require induction, making them difficult to detect with traditional susceptibility tests. Examples include hVISA [84], inducible clindamycin resistance (D-test) [87], and some weakly hydrolytic carbapenemases like OXA-48 [88], which can lead to false-negative results and undetected resistant subpopulations. Furthermore, phenotypic methods reveal only the presence of resistance, not the underlying mechanism, limiting their utility for epidemiological surveillance, infection control, and understanding how resistance genes are transmitted between strains or species [18].

3.2. Molecular Detection Methods: Polymerase Chain Reaction

To complement phenotypic AST, molecular diagnostic techniques, particularly polymerase chain reaction (PCR) based genotypic methods, have been developed for the direct detection of known resistance genes [89]. These methods reduce detection time from days to hours, offer superior sensitivity and specificity for targeted genes, and obviate the need for viable organisms [14]. They also enable predictive resistance monitoring before phenotypic changes appear and improve the efficiency of large-scale screening through high-throughput and automated workflows [90].

Conventional PCR remains the foundational genotypic approach for AMR detection [91]. It involves amplifying specific DNA targets through thermal cycling, such as *mecA*, *vanA/B* [92], followed by visualization of the amplified product via gel electrophoresis. This method is straightforward, cost-effective to establish, and suitable for single-target detection in well-equipped basic laboratories. However, it provides only qualitative results, is prone to amplicon carryover contamination, and cannot quantify target copy number.

Real-time quantitative PCR (qPCR) monitors amplification in real time via fluorescent probes or intercalating dyes [93]. The accumulation of fluorescence is monitored cycle-by-cycle, allowing for real-time quantification of the initial target amount. qPCR offers rapid turnaround (1.5–2.5 h), reduced contamination risk compared to conventional PCR, and quantitative output. Limitations include reliance on calibration curves, higher costs, and susceptibility to inhibition by complex clinical matrices (e.g., blood, sputum), which can compromise quantification accuracy [94].

Multiplex PCR enables simultaneous detection of multiple resistance targets in a single reaction, typically using multiple primer sets and probe systems labeled with different fluorophores [95]. This approach is central to many commercial syndromic panels. It maximizes information yield from limited sample material, improves workflow efficiency, and is ideal for screening a defined set of common resistance determinants. Challenges include complex assay design to minimize primer interference and ensure balanced amplification efficiency across targets, occasionally at the cost of reduced sensitivity for individual genes relative to singleplex assays.

Digital PCR (dPCR) represents a more recent advance, partitioning the PCR reaction into thousands to millions of individual nanoliter-volume compartments such that each contains zero, one, or few target molecules [96]. Following endpoint amplification, each compartment is scored as positive or negative, allowing absolute

quantification of target copy number using Poisson statistics without requiring external calibration standards. dPCR offers exceptional precision, sensitivity for low-abundance targets, and high tolerance to PCR inhibitors. However, broader adoption is limited by higher per-test costs, lower throughput than qPCR, and requirement for dedicated instrumentation.

Despite these advances, molecular genotypic methods share fundamental limitations that create two interdependent diagnostic gaps. First, PCR is inherently limited to detecting targets for which primers have been designed; it cannot identify novel resistance mutations or previously uncharacterized resistance genes [17]. This coverage gap is particularly concerning given the continuous evolution of β-lactamases and other resistance determinants. Second, the detection of a resistance gene does not guarantee its expression, nor does it reveal the quantitative level of enzymatic activity or the resulting MIC [97]. A strain may harbor a blaKPC gene that produces insufficient carbapenemase to confer clinical resistance, or, conversely, a strain may be phenotypically resistant through the synergistic effect of a low-level enzyme plus an overexpressed efflux pump plus a porin deficiency—a cumulative mechanism invisible to single-gene or even multiplexed detection panels [19]. This genotype-to-phenotype discordance constitutes the interpretive gap.

3.3. Three Diagnostic Gaps

The limitations of phenotypic and molecular methods (Table 1) define three critical diagnostic gaps: temporal gap, mechanistic gap, and interpretive gap. Culture-based AST is precise but prohibitively slow. Molecular tests are rapid but blind to unknown mutations and cannot capture functional enzyme activity or multi-mechanism synergy. Most critically, neither paradigm alone can reliably predict the quantitative, clinically meaningful resistance phenotype from genotypic or single-parameter data. Section 4 examines how the integration of advanced functional materials and artificial intelligence is systematically addressing each of these gaps.

Table 1. Limitations of Traditional and Molecular Bacterial Antimicrobial Resistance Detection Methods.

Method Name	Time Required	MIC Determination	Culture Required	Sensitivity/ Specificity	Operational Complexity	Cost	Key Limitations
Broth Microdilution [8,71,72]	18–24 h	Quantitative (direct MIC readout)	Yes	High/High (Gold Standard)	High	Low reagent cost; higher for commercial systems	Labor-intensive, difficult to detect contamination/inoculum viability issues.
Disk Diffusion (Kirby-Bauer) [9,75,76]	16–18 h	Semi-quantitative (interpreted via breakpoints)	Yes	Moderate/Moderate	Low	Low	Provides only qualitative/semi-quantitative results.
Gradient Diffusion (Etest) [77–79]	18–24 h	Quantitative (direct MIC readout)	Yes	High/High	Moderate	High	Higher per-test cost, occasional MIC deviations.
Automated AST Systems [11,83,84]	4–18 h	Quantitative/ Categorical	Yes	High/High	Low	High	High initial investment and maintenance, limited drug selection on panels.
Conventional PCR [91,92]	4–6 h	No MIC (detects gene presence only)	No	Moderate/High	Moderate	Low	Qualitative; contamination-prone; no quantification.
Real-Time Quantitative PCR (qPCR) [93,94]	1.5–2.5 h	No MIC (detects gene presence only)	No	High/High	Low to Moderate	Medium to High	Requires calibration; higher cost; susceptible to PCR inhibitors.
Multiplex PCR [95]	1.5–2.5 h	No MIC (detects gene presence only)	No	High/High	Moderate	Medium to High	Complex design/optimization; potential primer interference.
Digital PCR (dPCR) [96]	3–4 h	No MIC (detects gene presence only)	No	High/High	Moderate	High0	High cost; lower throughput; requires specialized equipment.

4. Emerging Functional Materials: Bridging Diagnostic Gaps through Rational Design

The preceding section established that the clinical management of antimicrobial resistance is critically hampered not by a single deficiency, but by three interdependent diagnostic gaps. Addressing these gaps requires moving beyond incremental improvements to existing culture-based or PCR-based workflows. It demands a fundamental rethinking of the detection event itself, shifting the analytical focus from the relatively slow biological processes of bacterial growth or thermal cycling to the rapid, intrinsic physical or chemical properties of purpose-designed materials.

This section examines how emerging functional materials are enabling this shift. The diagnostic power of these materials is not monolithic; it arises from a two-tiered innovation. The first tier is the material itself, with its precisely engineered structural, optical, electronic, or catalytic properties at the nanoscale. The second tier is the specific sensing architecture that translates these intrinsic properties into a measurable, quantitative signal upon interaction with a resistance biomarker (Figure 2). It is this translation, from a material's fundamental physics or chemistry to a diagnostic readout, that enables capabilities previously unattainable, such as detecting a single active enzyme molecule in a complex biological fluid or monitoring the real-time formation of a drug-tolerant biofilm.

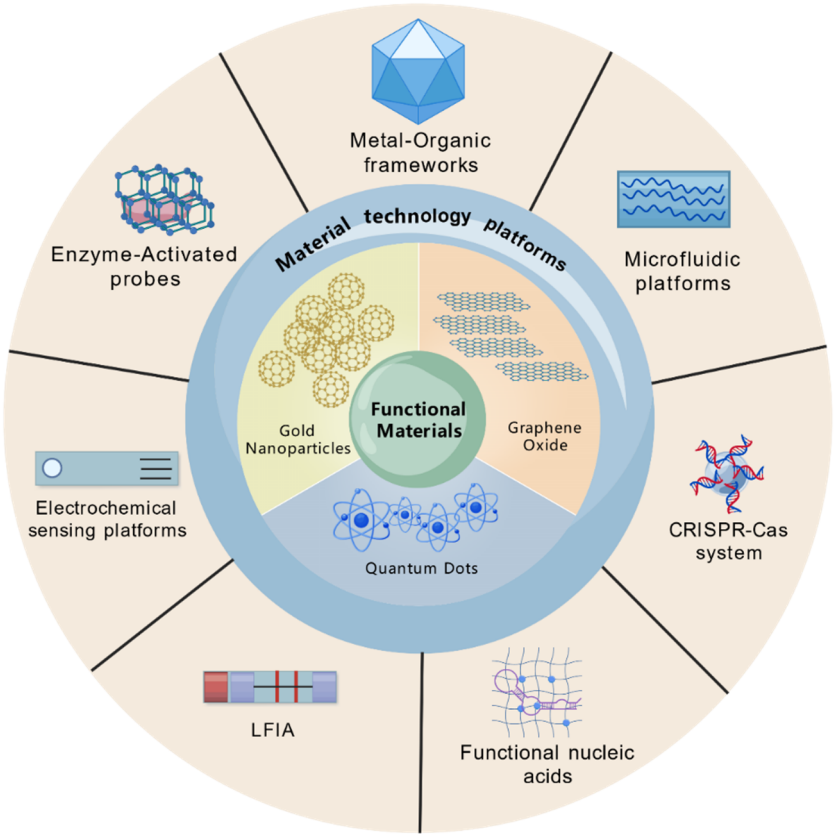

Figure 2. Summary of Functional Materials and Material Technology Platforms.

4.1. Nanomaterial-Based Signal Transduction Platforms

The outstanding performance of nanomaterial-based sensors originates from two fundamental properties: an exceptionally high specific surface area that enables dense immobilization of recognition elements [98], and unique optoelectronic properties that translate molecular interactions into measurable signals with high efficiency [99]. These materials circumvent the diffusion-limited kinetics of conventional assays, compressing detection times from days to minutes.

4.1.1. Gold Nanoparticles as Plasmonic Signal Transducers

Gold nanoparticles (AuNPs) exhibit localized surface plasmon resonance (LSPR), arising from collective oscillation of conduction band electrons in response to incident light. This oscillation generates an intense electromagnetic field confined to the nanoparticle surface, making the LSPR exquisitely sensitive to changes in the local dielectric environment, including interparticle distance, surface adsorption of biomolecules, and the refractive index of the surrounding medium [100]. Spherical AuNPs (20–40 nm) display a characteristic ruby-red color due to LSPR in the visible spectrum; aggregation red-shifts the peak, yielding a purple-blue coloration that can be detected by the naked eye or quantified spectrophotometrically [101].

A field-portable plasmonic biosensor exemplifies this application. In this platform, AuNPs were functionalized with thiol-modified oligonucleotide probes specific to the carbapenemase genes *blaNDM-1* and *blaOXA-1* [102,103]. When target DNA is present, hybridization between the nanoparticle-bound probes and complementary target sequences alters the interparticle distance, modulating the LSPR coupling and producing a visually detectable color change. The researchers demonstrated that a simple thermal lysis boiling method for

DNA extraction, which can be performed with a portable heat block, is fully compatible with this approach. The system achieved parallel detection of both unamplified resistance gene targets directly from bacterial colonies within 30 min and demonstrated 100% concordance with PCR results on a panel of 50 clinical isolates [104] (Figure 3A). By eliminating both the culture step and the PCR amplification step, this platform directly bridges the temporal gap and enables on-site screening in resource-limited settings.

4.1.2. Graphene Oxide as a Universal Fluorescence Quenching Platform

Graphene oxide (GO) is a two-dimensional carbon nanomaterial with a high density of oxygen-containing functional groups on its basal plane and edges. These groups confer excellent aqueous dispersibility while the extended sp^2 carbon network provides unique electronic properties [105]. In biosensing, GO functions as an efficient fluorescence quencher via Förster resonance energy transfer (FRET) [106] and photoinduced electron transfer (PET) [107]. Single-stranded nucleic acids and proteins adsorb strongly onto GO through π-π stacking interactions between aromatic amino acid residues or nucleobases and the graphitic domains, as well as through electrostatic and hydrogen-bonding interactions. This adsorption brings any tethered fluorophore into intimate contact with the GO surface, resulting in quenching efficiency exceeding 95% [108].

A sophisticated detection platform was engineered that exploits this quenching property to achieve amplification-free gene quantification. Transcription activator-like effectors (TALEs) are engineered DNA-binding proteins with a central repeat domain; each 33–35 amino acid repeat recognizes one nucleotide via two hypervariable repeat-variable diresidues (RVDs) [109] (Figure 3C). This modular architecture allows TALEs to be programmed to bind virtually any double-stranded DNA sequence with high affinity and specificity. TALE proteins specific to the tetracycline resistance gene *tetM* were conjugated to CdSe/ZnS core-shell quantum dots (QDs) with high quantum yield. In the absence of the target, the TALE-QD conjugates are adsorbed onto the GO surface and the QD fluorescence is completely quenched. Upon recognition and sequence-specific binding to the double-stranded *tetM* DNA, the TALE-QD complex undergoes a conformational change that reduces its affinity for GO, causing detachment and recovery of intense QD fluorescence (Figure 3B). This platform achieved a 1.2 femtomolar(fM) detection limit without DNA amplification, thereby eliminating PCR bias and enabling direct quantification of gene copy number [109]. The programmable nature of TALEs enables this platform to be rapidly adapted for detecting virtually any resistance gene sequence simply by redesigning the TALE repeat variable diresidues.

4.1.3. Quantum Dots as Superior Fluorescent Labels

Quantum dots are semiconductor nanocrystals, typically 2–10 nm in diameter, composed of elements from groups II–VI or III–V of the periodic table [110]. Their fluorescence arises from quantum confinement effects: when the nanocrystal size is smaller than the Bohr exciton radius, the energy levels become discrete and the bandgap increases with decreasing size. This confers optical properties superior to organic fluorophores: size-tunable, narrow emission (FWHM ~ 30–40 nm); broad absorption enabling multiplexed excitation; exceptional photostability; and high quantum yields with molar extinction coefficients 10–100-fold greater than organic dyes [111].

Capitalizing on the narrow, symmetric emission spectra of QDs, researchers developed a one-step fluorescent biosensor for multiplexed resistance gene detection using a nanocobalt porphyrin–dual QD system [112]. The sensing mechanism exploits the differential affinity of nanoCoTPyP toward single-stranded versus double-stranded DNA. Two QD populations with distinct emission wavelengths were each conjugated with ssDNA probes complementary to specific resistance gene targets. In the absence of target, nanoCoTPyP adsorbs onto the QD-ssDNA conjugates and efficiently quenches their fluorescence. Upon target hybridization, the resulting double-stranded DNA releases nanoCoTPyP, restoring intense QD fluorescence (Figure 3D). This homogeneous, separation-free design enables simultaneous quantification of two resistance genes within one hour, achieving detection limits of 24 pM and 20 pM for the respective targets, and was validated on clinical sputum specimens from patients with suspected multidrug-resistant tuberculosis. The principle is readily extensible to other resistance genes by redesigning the ssDNA probe sequences, directly bridging the mechanistic gap through multiplexed, amplification-free genotyping in a single reaction [113].

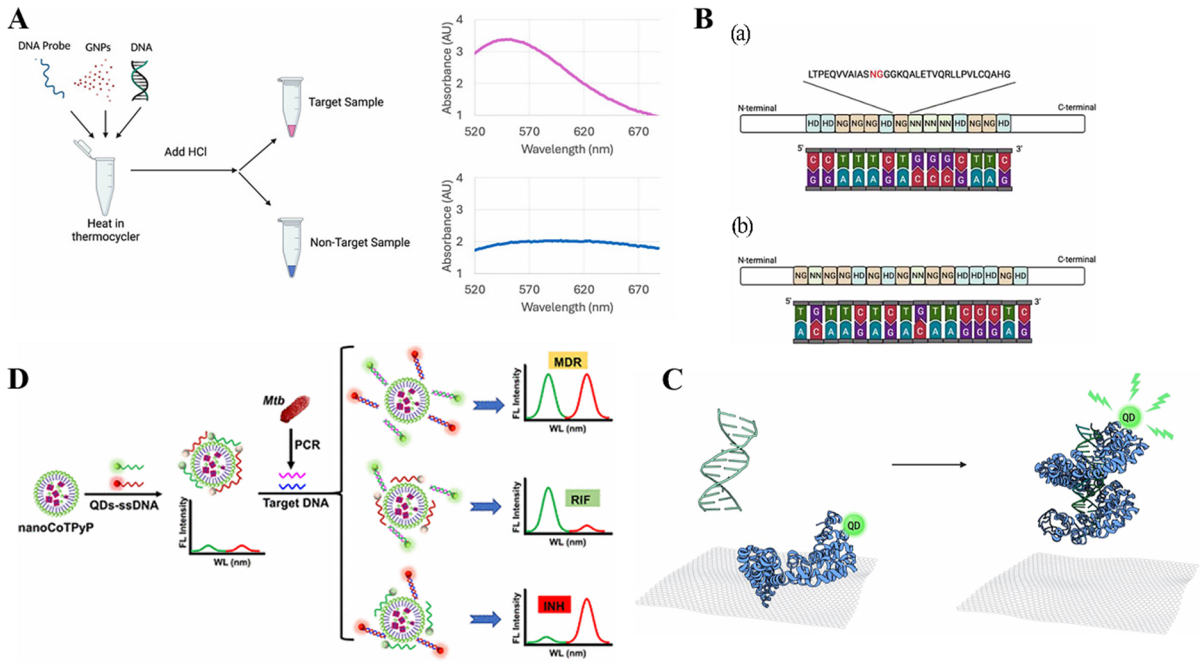

Figure 3. Nanomaterial-Based Signal Amplification and Transduction Platforms. (**A**) The principle of detecting target DNA sequences from Ref. [104]. Copyright 2025, MDPI. (**B**) Schematic representation of TALEs and GO-based biosensors for the detection of two different antibiotic resistance genes from Ref. [109]. Copyright 2023, American Chemical Society (ACS). (**C**) Sequence of RVDs and their respective target DNA sequence from Ref. [109]. Copyright 2023, American Chemical Society (ACS). (**D**) Principle of fluorescent biosensors for detecting multidrug resistance genes from Ref. [112]. Copyright 2022, American Chemical Society (ACS).

4.2. Metal-Organic Frameworks and Covalent Organic Frameworks

Metal-organic frameworks (MOFs) are crystalline, porous coordination polymers assembled from metal ions or clusters connected by polytopic organic linkers through coordination bonds. This modular construction affords unprecedented structural and chemical tunability: the pore size, shape, and internal surface functionality can be systematically engineered by selecting from a vast library of metal nodes and organic linkers. MOFs exhibit exceptional specific surface areas, typically 1000–7000 m^2/g with some exceeding 10,000 m^2/g, and tunable pore volumes accommodating guests ranging from small gases to macromolecules. The ordered arrangement of metal centers provides well-defined single-site catalysis; additionally, some MOFs exhibit intrinsic nanozyme activity stemming from coordinatively unsaturated metal sites that function as Lewis acids or redox centers [114,115]. Covalent organic frameworks (COFs) are an analogous class of crystalline porous materials constructed entirely from light elements connected through strong covalent bonds. COFs possess highly ordered, extended π-conjugated frameworks that facilitate charge carrier transport, and their pore environment can be engineered with atomic precision by incorporating functional groups into the organic building blocks before framework synthesis [116].

Self-cascading MOF@MOF nanozyme systems represent a transformative advance, confining multi-enzyme cascade reactions within a single nanostructure [117]. The conceptual innovation lies in spatially segregating two distinct catalytic activities into an outer shell and an inner core, such that the product of the first enzymatic reaction becomes the substrate for the second, achieving signal amplification through sequential catalytic turnover. In one design, a zirconium-based MOF shell with glucose oxidase-mimetic activity was grown epitaxially around an iron-based MOF core with peroxidase-like activity. The outer shell first catalyzes the oxidation of glucose to gluconic acid with concomitant generation of H_2O_2, which then diffuses through the porous shell into the inner core, where the peroxidase-mimetic MOF catalyzes the H_2O_2-mediated oxidation of a chromogenic substrate such as 3,3′,5,5′-tetramethylbenzidine to produce a strongly colored product [118]. When further functionalized with an aptamer or antibody that selectively captures β-lactamase, the binding event modulates the catalytic activity through steric or allosteric effects, providing a quantitative readout of enzyme concentration. This cascading process converts a single molecular recognition event into thousands of signaling molecules, achieving femtomolar detection limits for β-lactamase with a linear dynamic range spanning six orders of magnitude [119] (Figure 4A). The critical advance here is that the system quantifies the specific enzymatic activity rather than merely detecting the presence of the enzyme, providing functional resistance profiling unattainable by traditional AST or PCR.

Building on the catalytic advantages of MOFs, a core-shell architecture integrating a MOF core with a COF shell was developed to create a multi-functional bacterial sensing platform [120]. The FeNi-MOF core provides magnetic responsiveness for facile separation and concentration of captured bacteria from complex clinical samples such as blood culture broth or urine [121,122]. The COF shell, functionalized with boronic acid groups through post-synthetic modification, serves a dual purpose: the extended π-conjugated framework facilitates strong, multivalent binding to bacterial surface glycoproteins through a combination of boronate-diol covalent bonding, hydrophobic interactions, and π-π stacking, while the high surface area also adsorbs and concentrates small-molecule fluorescent substrates [123]. When aptamers specific to surface markers of multidrug-resistant bacteria are further immobilized onto the COF shell, a recognition-capture-signal amplification cascade is established (Figure 4B). Using fluorescence detection, this platform achieved detection limits of 2 CFU/mL for *Acinetobacter baumannii* and 3 CFU/mL for *Pseudomonas aeruginosa* in spiked urine samples, with a dynamic range of 10–10^8 CFU/mL. The sensor showed negligible cross-reactivity with non-target species and exhibited less than 5% signal variation in the presence of a 100-fold excess of common interfering substances. By rationally designing the MOF-COF interface at the molecular level, the system achieves both the ultrasensitive detection limit needed for early-stage infection diagnosis and the specificity to distinguish the infecting pathogen from normal flora in a complex polymicrobial clinical sample [124].

4.3. Enzyme-Activated Probes for Functional Resistance Imaging

Traditional methods for detecting β-lactamase activity rely on indirect endpoints: growth in the presence of a β-lactam antibiotic or detection of the *bla* gene by PCR [125]. Both fail to provide spatiotemporal information about where and when the enzyme is active within an infection site [126]. Enzyme-activated near-infrared (NIR) fluorescent probes represent a fundamentally different class of materials that directly convert enzymatic activity into an imaging signal *in situ*. The design involves covalently linking a fluorophore to an enzyme substrate such that its emission is initially quenched via photoinduced electron transfer (PET), Förster resonance energy transfer (FRET), or internal charge transfer (ICT). Enzymatic cleavage of the substrate removes the quenching moiety or alters the fluorophore's electronic structure, resulting in a dramatic fluorescence turn-on [127].

The probe CNIR5 illustrates the multi-effect design strategy [127,128]. In its native state, CNIR5 is dark (nonfluorescent) due to PET from a quencher to the fluorophore. Upon β-lactamase-mediated hydrolysis, three concerted events are triggered. First, cleavage eliminates the quenching pathway, restoring strong NIR fluorescence from the cyanine-derived fluorophore. Second, the cleavage reaction unmasks a hydrophobic alkyl chain, causing the activated fluorophore to undergo a spontaneous phase transition from the aqueous extracellular environment to the lipophilic bacterial membrane. Third, the unmasked moiety contains an electrophilic group that reacts with nucleophilic amino acid residues on bacterial surface proteins, covalently immobilizing the fluorophore at the infection site and preventing diffusion away from the target [129–131]. This multi-response mechanism solves the fundamental problem of *in vivo* probe washout and nonspecific redistribution that plagued earlier designs. In a murine pulmonary tuberculosis model, CNIR5 enabled detection of 10^4 CFU, surpassing the sensitivity of conventional fluorescent probes by approximately one order of magnitude [128] (Figure 4C). Iterative optimization led to CNIR800, capable of detecting bacterial loads $<10^3$ CFU in a murine thigh infection model [132] (Figure 4D).

This technology enables *in vivo* discrimination between enzyme-producing resistant infections and susceptible counterparts. When mice bearing both a drug-resistant *E. coli* infection in the right thigh and a drug-sensitive E. coli infection in the left thigh were injected with CNIR800, a strong NIR fluorescence signal was observed exclusively from the resistant infection with a target-to-background ratio exceeding 10:1, while the sensitive infection showed signal identical to sterile inflammation controls. This specificity in pinpointing the functional mechanism of resistance directly *in vivo* is a diagnostic capability that fundamentally transcends both culture-based AST, which would report both infections identically based on planktonic MIC, and PCR, which would only report gene presence without confirming whether the enzyme is functional [132]. Furthermore, this design paradigm has been extended to multimodal imaging through the probe BIN-3, which incorporates a trans-cyclooctene moiety that becomes available for bioorthogonal click chemistry with tetrazine-modified reporters upon β-lactamase activation. By administering BIN-3 first to accumulate at the infection site and a panel of tetrazine reporters in a second injection, multi-scale imaging from whole-body PET/CT localization to high-resolution optical imaging of the infection margin is achieved using a single molecular trigger [133].

Despite promising preclinical performance, NIR probes face significant hurdles to clinical translation. The tissue penetration depth of NIR-I light is limited to approximately 1–3 cm, restricting utility for deep-seated infections. Although NIR-II probes offer deeper tissue penetration, their clinical development remains in early stages. The

regulatory pathway for an enzyme-activatable imaging agent combined with a fluorescent endoscope or intraoperative imaging system remains undefined; no β-lactamase-activated probe has yet entered clinical trials [134].

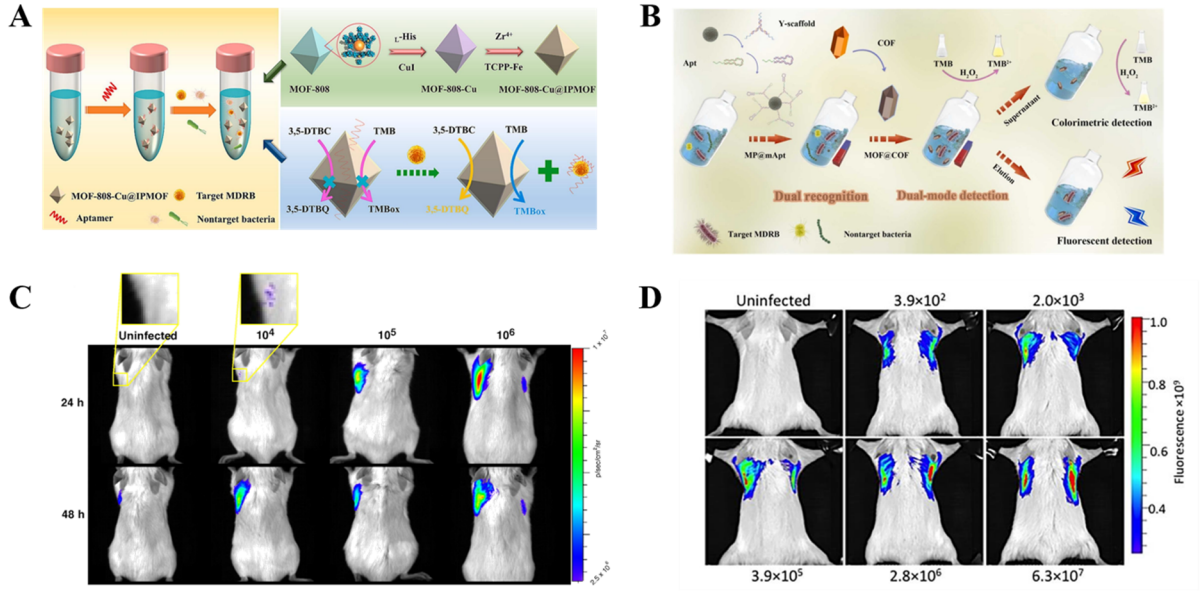

Figure 4. Advanced Materials for Enzyme Activity-Based Sensing and In Vivo Imaging: Bridging the Temporal and Mechanistic Gaps. (**A**) MOF@MOF nanozyme for detection of multidrug-resistant bacteria from Ref. [119]. Copyright 2025, Elsevier. (**B**) Dual-mode biosensing platform for MDRB detection from Ref. [120]. Copyright 2024, Elsevier. (**C**) Imaging of mice body and administered the indicated CNIR substrate from Ref. [128]. Copyright 2010, National Academy of Sciences. (**D**) Imaging of mice body from Ref. [132]. Copyright 2017, Oxford University Press.

4.4. Electrochemical Sensing Platforms

Electrochemical biosensors transduce biological recognition events into a measurable electrical signal through amperometry, potentiometry, or electrochemical impedance spectroscopy (EIS). The core of these sensors is the electrode material and its surface modification, which together determine sensitivity, selectivity, and stability [135].

A transformative advance in electrode design is the integration of three-dimensional porous architectures. A 3D hydrogel-paper scaffold electrode was developed for β-lactamase detection by combining a flexible cellulose paper substrate with a highly absorbent, conductive hydrogel matrix composed of polyacrylamide-co-acrylic acid doped with polyaniline [136]. This design circumvents the planar electrode trade-off between miniaturization and surface area by expanding the sensing interface into three dimensions. The interconnected macroporous network of the hydrogel-paper composite, with pore sizes of 10–200 μm, increases the effective surface area by two to three orders of magnitude compared to a flat gold electrode of the same geometric footprint, dramatically enhancing the loading capacity for immobilized antibodies. The conductive polymer backbone facilitates electron transfer, while the hydrogel's high water content maintains the native conformation and activity of the immobilized biomolecules [137]. For detection, anti-β-lactamase antibodies are covalently immobilized within the 3D scaffold. When a clinical sample is applied, β-lactamase in the sample diffuses through the porous network and binds to the immobilized antibodies. This binding event alters the interfacial charge distribution; specifically, the accumulation of a negatively charged protein layer at the electrode-solution interface increases the charge transfer resistance and decreases the double-layer capacitance. These changes are monitored in real time by EIS, with the shift in charge transfer resistance being proportional to the β-lactamase concentration over a 4-log dynamic range (Figure 5A). The entire detection process is completed within 15–20 min, a timeframe that directly bridges the temporal gap and is compatible with clinical decision-making for sepsis management [138].

Further sensitivity enhancement is achieved by incorporating nanomaterials into the electrode matrix. Gold nanoparticle-reduced graphene oxide (AuNP-rGO) composites, electrodeposited onto screen-printed carbon electrodes (SPCEs), provide a conductive, high-surface-area scaffolds. The AuNPs serve as anchor points for thiol-modified oligonucleotide probes or cysteine-tagged proteins, while the rGO network ensures efficient electron transfer. When a β-lactam antibiotic is immobilized onto this nanocomposite as a substrate for β-lactamase, the enzyme's hydrolysis of the β-lactam ring can be monitored via differential pulse voltammetry by measuring the change in redox current from a ferri/ferrocyanide probe in solution [139]. This approach achieves nanomolar

detection limits for clinically relevant carbapenemases. A multi-electrode array functionalized with cephalosporin substrates of varying hydrolysis susceptibilities generates fingerprint-like hydrolysis profiles that discriminate among β-lactamase classes. For instance, Class A carbapenemases such as KPC produce a distinctly different hydrolysis profile from Class B metallo-β-lactamases such as NDM and VIM [140]. This provides real-time functional enzyme classification, bridging the mechanistic gap without requiring gene sequencing.

Electrochemical sensors face the persistent challenge of biofouling when applied to direct clinical sample testing [141]. The nonspecific adsorption of proteins, lipids, and cells from complex matrices such as whole blood or sputum onto the electrode surface increases the background impedance, masks the specific signal, and can cause progressive sensor drift. Strategies to mitigate biofouling, including zwitterionic polymer coatings, nanoporous protective membranes, and pulsed electrochemical cleaning protocols, are under active investigation but have yet to be validated in large-scale, multi-center clinical studies with unprocessed clinical specimens.

4.5. Lateral Flow Immunoassay Enhanced by Advanced Materials

Lateral flow immunoassays (LFIAs) are the most widely deployed point-of-care diagnostic format, valued for their operational simplicity, rapid results, low cost, and ambient temperature stability [142–144]. Standard LFIAs employ 20–40 nm spherical AuNPs as colorimetric reporters [145]. In a typical sandwich format, AuNPs are conjugated with a detection antibody and a second capture antibody is immobilized at the test line. When a liquid sample containing the target analyte flows through the strip by capillary action, the antibody-AuNP conjugate binds the analyte and the resulting complex is captured at the test line, forming a visible red line whose intensity is ideally proportional to the analyte concentration. The fundamental limitation of this format is sensitivity: the visual detection threshold for the human eye is approximately 1–10 ng/mL for a protein target under optimal conditions, often an order of magnitude too high for clinically relevant concentrations of resistance biomarkers [146].

Laser-synthesized platinum and platinum-gold alloy nanoparticles have markedly enhanced LFIA performance [147]. Femtosecond-laser ablation in liquid is a physical synthesis method wherein high-intensity, ultrafast laser pulses are focused onto a high-purity metal target immersed in ultrapure water. The extreme localized energy density vaporizes and ionizes the metal surface, generating a plasma plume that rapidly quenches and condenses into nanoparticles [148]. This process offers two decisive advantages over conventional chemical reduction: it yields nanoparticles with a clean, surfactant-free surface that exhibits higher catalytic activity, and it enables the facile synthesis of alloy nanoparticles with precisely controlled composition simply by using an alloy target. In LFIA applications, these Pt-Au alloy nanoparticles generate dual-mode signals. The Au component retains the LSPR absorption that provides the baseline plasmonic red color at the test line, while the Pt-rich surface possesses intrinsic peroxidase-like catalytic activity. Following the LFIA run, the strip is briefly immersed in a chromogenic substrate solution (e.g., TMB). The Pt-Au nanoparticles captured at the test line catalyze the oxidation of the substrate, depositing an intensely colored, insoluble precipitate that dramatically amplifies the visual and instrumental signal by a factor of 10–100 compared to the plasmonic color alone [149].

The analytical advantage of this material innovation is fully realized when combined with machine learning-based image analysis. A supervised machine learning model was trained on a dataset of over 5000 test-line images acquired under standardized illumination from strips tested with known concentrations of recombinant CMY-34 β-lactamase. The trained model learned to extract and jointly weight multiple image features—including grayscale textural patterns, color channel ratios, and spatial uniformity of the test line—that are collectively diagnostic of target concentration but imperceptible to the human eye. When applied to a blinded validation set, the AI-enhanced analysis of Pt-Au alloy LFIA strips achieved a detection limit of 1 ng/mL for CMY-34, representing an approximately 10-fold improvement over visual interpretation of the same strips and comparable to laboratory-based ELISA [147,149]. This integration of an advanced catalytic nanomaterial with machine learning-based signal interpretation transforms a qualitative yes/no LFIA into a quantitative, instrument-read diagnostic, bridging both the temporal gap through rapid turnaround and the interpretive gap through objective quantification.

4.6. Functional Nucleic Acids as Programmable Recognition Elements

Functional nucleic acids, specifically aptamers and DNAzymes, constitute a distinct class of programmable recognition elements spanning synthetic chemistry and molecular biology. Unlike antibodies or enzymes, these nucleic acid-based recognition elements are generated entirely in vitro through systematic evolution of ligands by exponential enrichment (SELEX), enabling the isolation of sequences that bind with high affinity and specificity to virtually any target, including small-molecule antibiotics, metal ions, whole bacterial cells, and specific resistance enzymes [150]. Once identified, functional nucleic acids can be chemically synthesized with high purity,

site-specifically modified with fluorophores, quenchers, or electrochemical tags, and integrated into a virtually unlimited range of sensing architectures. This programmability makes them ideal building blocks for customizable AMR biosensors [151].

A kanamycin A-specific aptamer was integrated into a signaling-probe displacement electrochemical aptamer-based (SD-EAB) sensor [152]. In this design, a thiolated, methylene blue-tagged aptamer is self-assembled onto a gold electrode surface. In the absence of the target, the aptamer adopts a partially folded conformation that positions the methylene blue (MB) redox reporter in proximity to the electrode surface, facilitating efficient electron transfer and producing a high baseline current. Upon binding kanamycin, the aptamer undergoes a binding-induced conformational change, typically a folding or compaction event, that increases the distance between the methylene blue tag and the electrode, decreasing the electron transfer rate and producing a measurable drop in current. This sensor achieved a detection limit of 20 nM for kanamycin in buffer, with a response time of less than 5 min [153].

The true advance of this platform lies not merely in its sensitivity, but in its ability to distinguish between the active antibiotic and its enzymatically inactivated form. Aminoglycoside-modifying enzymes acetylate, phosphorylate, or adenylylate specific functional groups on the aminoglycoside scaffold. These covalent modifications alter the molecular shape and hydrogen-bonding capacity of the antibiotic, consequently disrupting its binding to the aptamer. By measuring the aptamer-binding signal before and after incubation with a bacterial lysate, the sensor can directly quantify AME activity—the functional resistance mechanism—in a manner analogous to the MOF-nanozyme platforms described earlier but using a purely nucleic acid-based recognition element. This functional readout bridges the mechanistic gap that PCR cannot address [153].

While aptamer-based sensors have been extensively demonstrated in academic laboratories, their translation to real clinical samples faces hurdles common to many material-based platforms. The nuclease-rich environment of biological fluids rapidly degrades unprotected nucleic acid aptamers, limiting sensor lifetime unless chemically modified nucleotides with 2′-O-methyl or phosphorothioate backbones are incorporated [154]. Aptamer affinity, while often excellent in selection buffer, can be reduced by orders of magnitude in the complex ionic and proteinaceous environment of clinical samples. Furthermore, the SELEX process itself remains time-consuming and costly.

4.7. CRISPR-Cas Systems for Programmable, Ultra-Specific Gene Detection

CRISPR-Cas systems have transformed molecular diagnostics by enabling a programmable, RNA-guided detection of specific nucleic acid sequences with single-base resolution [155]. Cas12a and Cas13a effectors proteins function as follows: a CRISPR RNA guides the nuclease to its target sequence through Watson-Crick base pairing. Upon target recognition, the nuclease undergoes a conformational change that allosterically activates a potent, non-specific trans-cleavage activity. The activated nuclease then indiscriminately cleaves any nearby single-stranded DNA (for Cas12a) or RNA (for Cas13a) reporter molecules that are labeled with a fluorophore-quencher pair, separating the two and generating a fluorescence signal amplified by the multiple-turnover nature of the catalytic cleavage. This mechanism provides a powerful combination of sequence specificity, since the crRNA can be designed to span a single nucleotide polymorphism, and signal amplification, since a single target recognition event triggers the cleavage of thousands of reporter molecules [156].

Integration of CRISPR-Cas12a with a rationally designed 3D DNAzyme yielded a fully instrument-free colorimetric platform for resistance gene detection [157]. The 3D DNAzyme is a self-assembled, G-quadruplex-based nanostructure that, upon binding hemin, exhibits peroxidase-mimicking catalytic activity capable of oxidizing colorless substrates to intensely colored products visible to the naked eye. The DNAzyme is purposefully designed to contain an internal single-stranded DNA linker that serves as the preferred substrate for the Cas12a trans-cleavage activity (Figure 5B). In the operational workflow, extracted bacterial DNA is incubated with a pre-assembled Cas12a-crRNA ribonucleoprotein complex targeting the *blaKPC* gene. If the target sequence is present, the activated Cas12a cleaves the 3D DNAzyme's catalytic core, inactivating it and preventing the subsequent color development upon substrate addition, producing a signal-off response. If the target is absent, the DNAzyme remains intact and produces a strong blue color [158].

CRISPR systems have also been hybridized with material-based signal enhancement to achieve detection limits relevant for clinical samples without pre-amplification [159]. Cas13a collateral cleavage products have served as triggers for the aggregation of ssDNA-functionalized gold nanoparticles, inducing a plasmonic color change easily visible by the naked eye. Alternatively, CRISPR-generated cleavage fragments release electrochemical tags from quantum dot-functionalized electrode surfaces, enabling attomolar-level detection with a portable potentiostat [160].

These material-CRISPR hybrids directly bridge both the temporal gap, with results in under one hour, and the interpretive gap, by discriminating between genetic variants with different clinical implications.

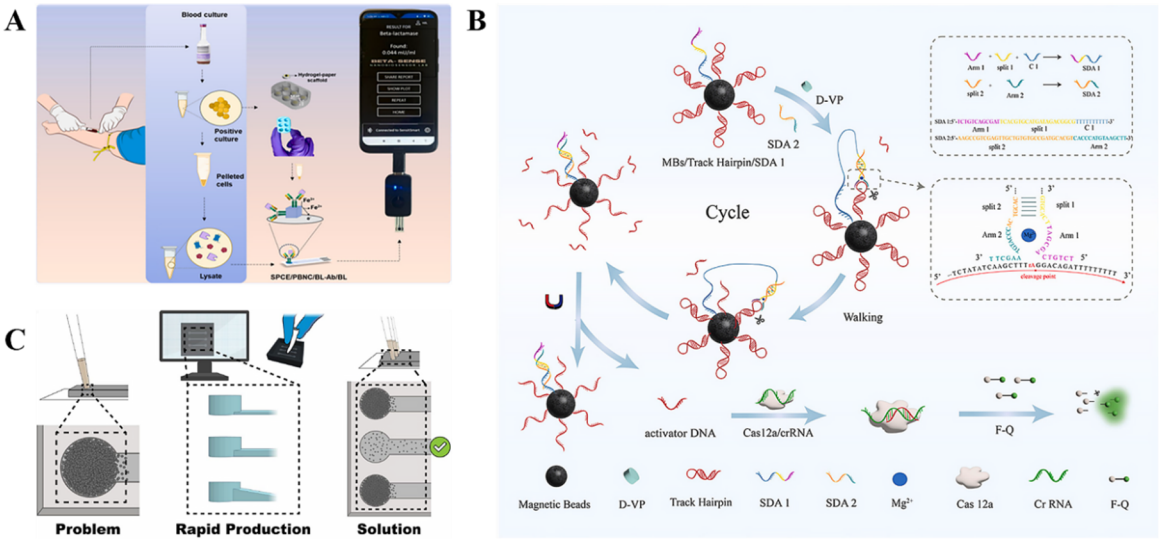

Figure 5. Integrated Diagnostic Platforms: Electrochemical, CRISPR, and Microfluidic Strategies for Comprehensive Resistance Profiling. (**A**) A highly sensitive PBNC integrated portable electrochemical detection platform from Ref. [138]. Copyright 2025, Elsevier. (**B**) An aptasensor coupled with CRISPR-Cas12a for the detection from Ref. [157]. Copyright 2025, Elsevier. (**C**) Rapid prototyping of microfluidic device features using stereolithographic 3D printing from Ref. [161]. Copyright 2025, Cold Spring Harbor Laboratory.

4.8. Microfluidic Platforms for Dynamic Biofilm Monitoring

Microfluidic chips enable an *in situ*, dynamic analysis platform for biofilm research by simulating biological microenvironments [162–164]. Their material selection directly influences the manufacturing process and detection performance. Polydimethylsiloxane (PDMS), due to its good gas permeability, biocompatibility, and elasticity, has become the primary substrate material for microfluidic chips [165]. PDMS-based microfluidic devices can resolve four distinct biofilm growth stages via real-time impedance monitoring: initial adhesion (0–6 h), microcolony formation (6–12 h), accelerated EPS secretion (12–18 h), and biofilm maturation (18–24 h). Acrylonitrile butadiene styrene (ABS) 3D-printed sacrificial molds combined with PDMS casting enable simple, low-cost microchannel fabrication [161]. This process does not require a cleanroom environment, lowers device costs, and offers the possibility of integrating biodegradable materials (Figure 5C).

The revolutionary capability of this platform lies in its ability to continuously monitor these transitions. By introducing an antibiotic at a specific stage and tracking the subsequent impedance response, the system can quantify whether the antibiotic kills planktonic bacteria, prevents biofilm initiation, penetrates and disrupts a pre-formed mature biofilm, or has no effect on the biofilm state. These functional parameters are entirely inaccessible to conventional AST yet are critical for predicting clinical treatment success [166]. A deep learning model based on a 1D convolutional neural network trained on raw impedance spectra from multiple *Pseudomonas aeruginosa* biofilms achieved over 95% accuracy in classifying the biofilm growth stage in real time, far surpassing the performance of manual equivalent circuit fitting [167]. This technology, by providing a direct, quantitative readout of the biofilm tolerance phenotype, directly bridges the interpretive gap where planktonic AST falsely predicts susceptibility.

Current limitations include the requirement for cleanroom photolithography to fabricate PDMS chips with embedded microelectrodes—a significant barrier in cost and technical expertise. Biofouling of the electrodes by components of complex clinical samples such as whole blood or sputum also remains a challenge, as the nonspecific adsorption of proteins and cells onto the electrode surface obscures the specific biofilm-derived signal.

5. AI-Enabled Intelligent Analytics: From Signal Decoding to Phenotype Prediction

The functional materials and sensing platforms described in Section 4 generate a wealth of high-dimensional, complex data—from time-resolved impedance spectra of biofilm growth to fluorescence kinetic traces of enzyme catalysis and multiplexed spectral barcodes of resistance genes. Traditional analytical methods, which rely on manual thresholding, peak fitting, or simple linear calibration curves, are fundamentally inadequate for extracting the full diagnostic information embedded within these datasets. They cannot, for example, automatically

distinguish subtle, multi-parametric patterns that characterize different resistance mechanisms, nor can they integrate heterogeneous data types to make a unified prediction of the resistance phenotype. AI, particularly its machine learning and deep learning subfields, has therefore emerged as the essential analytical core that bridges the gap between raw material-generated data and clinically actionable understanding [168]. This section systematically examines how specific AI architectures are being deployed across the diagnostic workflow: to enhance signal processing within individual biosensors, to fuse multi-modal data for quantitative resistance prediction, to guide the rational design of new sensing materials, and, increasingly, to enable decentralized, intelligent surveillance networks [169].

5.1. AI-Enhanced Signal Processing for Material-Based Biosensors

AI elevates material-based biosensors from qualitative or semi-quantitative tools to precise, operator-independent diagnostic instruments by extracting high-fidelity quantitative information from raw sensor outputs [170].

In lateral flow immunoassays (LFIAs), conventional visual inspection is inherently subjective. A supervised convolutional neural network (CNN) based on the ResNet-18 architecture was trained on over 5000 test-line images of the laser-synthesized Pt-Au alloy nanoparticle LFIA described in Section 4.5, representing known concentrations of recombinant CMY-34 β-lactamase. The CNN learned to extract hierarchical visual features—edges, textures, and spatial uniformity—using a regression objective to produce a continuous, quantitative output. As detailed in Section 4.5, this approach achieved a 10-fold sensitivity improvement over visual interpretation and a 3-fold improvement over conventional densitometry [147]. This transforms a rapid, low-cost LFIA into a quantitative point-of-care test delivering laboratory-level performance within 15 min.

For EIS-based biofilm monitoring (Section 4.8), a 1D-CNN trained directly on raw impedance spectra circumvented labor-intensive equivalent circuit modeling. Training labels were derived from consensus annotation by three microbiologists of time-lapse confocal microscopy images into four biofilm stages: reversible adhesion, microcolony formation, EPS secretion, and maturation. The 1D-CNN achieved >95% classification accuracy, substantially outperforming the best equivalent circuit-based approach (82%), while reducing analysis time from minutes to milliseconds [167]. This enables real-time, closed-loop biofilm monitoring and addresses the interpretive gap by providing a clinically meaningful phenotype from complex raw data.

5.2. AI-Driven Multimodal Data Fusion for Predictive Resistance Phenotyping

The central interpretive challenge is predicting the clinical resistance phenotype—the MIC—from heterogeneous data, as a single resistance gene rarely independently determines resistance levels [171].

A representative study on the prediction of carbapenem resistance in clinical *Klebsiella pneumoniae* isolates illustrates the value of AI-driven phenotype prediction. Using a dataset of 4367 *K. pneumoniae* genomes paired with meropenem MICs, researchers trained random forest and elastic net models on features derived solely from genome sequence data—including the presence of specific carbapenemase genes, porin gene mutations, and other genomic markers. The best-performing models achieved high accuracy for predicting clinical MIC categories directly from genotype [172]. Although this proof-of-concept was genome-centric, logical extensions incorporating functional enzyme kinetics (e.g., from MOF-nanozyme assays) and transcript-level porin expression data (e.g., *ompK35* from microfluidic dPCR) could substantially enhance predictive performance. Such multimodal fusion via ensemble methods (e.g., random forests) would be particularly valuable for resolving discordant cases—such as carbapenemase-positive isolates with low-level enzyme expression or compensatory permeability changes. Feature importance analysis in such a fused model would be expected to identify enzyme kinetic parameters as highly informative features, with molecular-level data refining predictions for borderline isolates. This framework exemplifies how materials science and AI integration can bridge the interpretive gap.

5.3. AI-Guided Rational Design of Sensing Materials

AI increasingly feeds back into material discovery. Graph neural networks (GNNs) have been trained on the CoRE MOF database, which contains over 14,000 experimentally synthesized structures. These models predict adsorption isotherms for small-molecule substrates—including β-lactam antibiotics—from pore geometry and chemical environment [173]. The trained GNN screened over 100,000 hypothetical MOF structures, identifying candidates with optimal pore sizes for cephalosporin substrates. Top-ranked candidates were synthesized and experimentally tested, yielding a significant correlation ($R^2 = 0.81$) between GNN-predicted binding affinity and experimentally measured sensor sensitivity. Generative approaches further expand design space: a generative adversarial network (GAN) designed novel antimicrobial peptide sequences that self-assemble into hydrogels with

4-fold higher binding affinity for drug-resistant *Staphylococcus aureus* compared to a rationally designed control, a strategy directly transferable to recognition layer design for bacterial biosensors [174].

5.4. AI for Decentralized Diagnostics and Global Surveillance

Edge AI enables point-of-care readers to operate independently of cloud connectivity [175]. As a representative direction, compressed deep learning models deployed on smartphones via frameworks such as TensorFlow Lite have been demonstrated for LFIA test line quantification, enabling accurate, quantitative AMR testing in primary care settings and remote field locations without the need for cloud connectivity [176]. Federated learning frameworks address data privacy and model generalization: AI models are trained locally on each diagnostic node and transmitting only anonymized model updates to a central aggregation server (Figure 6). This architecture enables a continuously improving, globally representative model while enabling real-time geospatial mapping of AMR trends for predictive outbreak analytics [177].

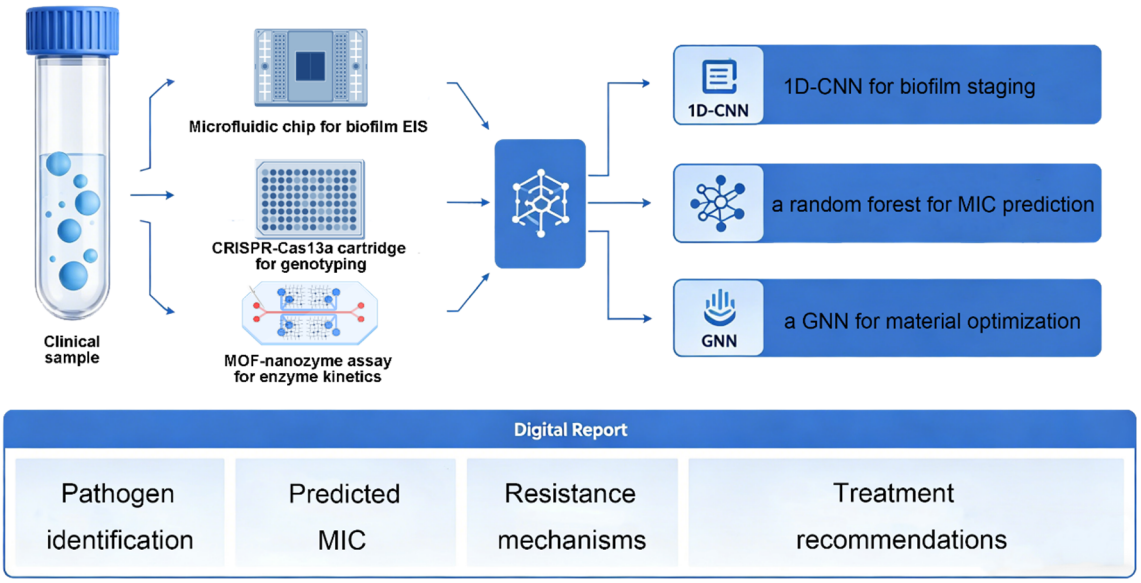

Figure 6. AI-Enabled Integrated Diagnostic Workflow for AMR.

5.5. Current Limitations and Future Challenges

Despite the compelling advances described, the integration of AI with material-based AMR diagnostics faces several significant hurdles that must be addressed for clinical translation [178]. The first is model generalizability and batch effects [179]. An AI model trained on data from a specific sensor batch, reagent lot, or clinical population may fail unpredictably upon deployment in different settings. This is a well-documented problem in the broader medical AI field, and robust domain adaptation and transfer learning methods must be developed to standardize AI model performance across diverse, real-world deployment conditions. The second challenge is explainability and clinical trust [180]. Clinicians are unlikely to base treatment decisions on a predicted MIC when the underlying model provides no interpretable justification for its output. Integrating explainability methods such as SHAP values and attention map visualizations into AI diagnostic tools can clarify which specific input features—for example, a particular enzyme kinetic parameter or the presence of a resistance gene—most strongly influenced a given prediction, thereby providing the auditable rationale that clinicians require. The third challenge relates to regulatory validation. Current regulatory frameworks (e.g., from the FDA or EMA) provide evolving but still incomplete guidance for AI-based diagnostic software, particularly for systems that combine a physical biosensor with a continuously updatable AI algorithm. The development of standardized validation protocols analogous to those for conventional AST (CLSI/EUCAST) is urgently needed to assess the accuracy, reproducibility, and clinical utility of AI-material hybrid diagnostics.

6. Integration Strategies, Clinical Translation, and Future Prospects

The path from laboratory demonstrations of material-AI hybrid diagnostics to clinical impact requires confronting interlocking technical, regulatory, economic, and logistical challenges.

6.1. Technical Reproducibility and Manufacturing Scalability

The exceptional performance of nanomaterials depends on precisely engineered structural features that are highly sensitive to synthesis parameters [181]. MOF nanozyme catalytic activity varies with solvothermal synthesis parameters; graphene oxide quenching efficiency depends on lateral size and defect density; gold nanoparticle plasmonic response is sensitive to size distribution. Achieving clinical-grade reproducibility requires a transition from manual, artisanal synthesis to scalable, quality-controlled manufacturing. Key enablers of this transition include continuous-flow microfluidic synthesis platforms and the establishment of certified reference materials analogous to those used by CLSI. Without such standardization, AI models trained on one batch will fail on another.

6.2. AI model Generalizability, Validation, and Explainability

The AI models described in Section 5 introduce their own set of translational challenges. A critical yet frequently overlooked problem is sensor-to-sensor transferability: a convolutional neural network trained to quantify test-line intensity on LFIA strips from one manufacturer will not necessarily perform accurately on strips from another, even if the nominal target and nanoparticle reporter are identical. Subtle differences in membrane porosity, antibody affinity, or nanoparticle size distribution generate image features imperceptible to the human eye yet sufficient to compromise model performance. Domain adaptation and transfer learning techniques, wherein a pre-trained model is fine-tuned on a small calibration dataset from the new sensor batch, represent a technical solution, but the routine deployment of these machine learning operations in a clinical laboratory setting remains an unresolved workflow challenge.

Equally pressing is the issue of model explainability [182]. A predicted MIC of 16 μg/mL for meropenem, generated by a random forest model fusing CRISPR genotyping, MOF-nanozyme enzyme kinetics, and digital PCR porin expression data, is an actionable clinical result. Clinicians require transparent prediction rationale to inform alternative therapeutic decisions. Explainable AI methods, such as SHAP values that decompose a prediction into the additive contribution of each input feature, and attention map visualizations for deep learning models, must be integrated to provide transparent and auditable outputs. Regulatory bodies are increasingly emphasizing algorithmic transparency in their evolving frameworks for Software as a Medical Device, and future clinical trials should incorporate standardized explainability metrics.

6.3. Biofouling, Sample Matrix Effects, and Direct Clinical Sample Testing

A recurring theme across the material platforms reviewed in Section 4 is the challenge of biofouling [183]. Sensor surfaces that deliver femtomolar detection limits in phosphate-buffered saline are confronted with entirely different environments in whole blood, sputum, or wound exudate. A fouling layer formed by the nonspecific adsorption of serum proteins, fibrinogen, and cellular debris elevates background noise, obscures target-specific signals, and induces progressive baseline drift. In electrochemical sensors, this proteinaceous layer impedes electron transfer [141]. In optical sensors, adsorbed proteins scatter light and autofluoresce [184]. In microfluidic channels, biofilm formation by non-target bacteria can confound impedance measurements [185]. Multiple anti-biofouling strategies are under investigation: zwitterionic polymer coatings form a tightly bound hydration layer that resists protein adsorption; nanoporous protective membranes physically separate the sensing interface from the bulk sample matrix; and pulsed electrochemical cleaning protocols can regenerate electrode surfaces *in situ*. However, these strategies have been validated predominantly using spiked or simplified samples. Demonstration of robust performance on large, diverse cohorts of unprocessed clinical specimens, and the integration of anti-fouling strategies into the initial sensor design, is a critical gating item for clinical translation.

6.4. Standardization, Regulatory Pathways, and Clinical Validation

Conventional AST operates within a mature standardization framework. CLSI and EUCAST publish definitive reference methods, establish quality control ranges for reference strains, and define interpretive breakpoints that translate MIC values into clinically meaningful categories [186]. No equivalent infrastructure exists for material-based or AI-augmented AMR diagnostics. The field currently lacks consensus on how to calibrate a MOF-nanozyme optical assay against reference broth microdilution, a standardized protocol for reporting confidence intervals on machine learning-predicted MICs, and inter-laboratory proficiency testing programs. Building this infrastructure will require concerted multi-stakeholder effort. As a minimum, any new diagnostic should report its essential agreement and categorical agreement against a prospectively collected, geographically diverse panel of clinical isolates. Although the U.S. FDA has issued guidance for AI-based

diagnostic software, the unique challenges posed by hybrid systems—in which variations in nanomaterial synthesis can shift the input data distribution seen by the AI model—remain inadequately addressed by current regulatory frameworks [187]. FDA Pre-Cert programs, which focus on the developer's quality management system, may offer a viable regulatory model.

6.5. Cost-Effectiveness and Deployment in Low- and Middle-Income Countries

The global burden of AMR disproportionately affects low- and middle-income countries (LMICs), where limited laboratory infrastructure, scarce trained personnel, and the high cost of diagnostics collectively impede clinical adoption [188]. A realistic assessment of total cost of ownership tempers enthusiasm for many platforms. Deploying a disposable CRISPR-based microfluidic cartridge demands a cold chain for reagent stability, a portable fluorescence reader for signal detection, and a reliable power supply—infrastructure that may not be available in all intended settings. Laser-synthesized platinum-gold alloy nanoparticles require a femtosecond laser system costing hundreds of thousands of dollars. Although the direct consumable cost of a single LFIA strip is minimal, the true per-test cost is dominated by amortized capital expenditures, skilled personnel, AI software licensing, and quality assurance programs. Genuinely deployable point-of-care AMR diagnostics for LMIC settings must be designed with these constraints as primary specifications. This favors equipment-free platforms, such as the CRISPR-3D-DNAzyme colorimetric sensor described in Section 4.7, or those leveraging ubiquitous smartphone infrastructure. Life-cycle cost analyses and health economic modeling comparing AI-material diagnostics to conventional AST in LMIC settings are urgently needed.

6.6. "One Health" Integration

AMR epitomizes the "One Health" challenge, as resistance genes and drug-resistant pathogens circulate continuously across human healthcare facilities, livestock production systems, aquaculture operations, and natural environmental reservoirs [189,190]. If successfully translated to field-deployable formats, the material-AI diagnostic platforms described in this review could create a unified, multi-sectoral surveillance network. A distributed network might include a portable CRISPR-based device detecting *bla*NDM-positive *E. coli* from a patient's urine in a rural clinic, an electrochemical biofilm sensor detecting biocide-tolerant *Salmonella* in a poultry processing facility, and a paper-based LFIA monitoring carbapenemase activity in river water downstream of a pharmaceutical manufacturing site. The AI models operating on the cloud platform would integrate these disparate data streams, perform geospatial cluster analysis, and issue risk-stratified alerts to public health agencies. Realizing this vision requires resolving substantial governance and data-sharing challenges. The WHO Global Antimicrobial Resistance and Use Surveillance System (GLASS) provides an existing infrastructure framework, but its scope is currently limited to phenotypic AST data. Integrating genotypic, functional, and AI-derived resistance data into the WHO GLASS platform—together with the development of harmonized data standards and ethical governance frameworks—should be regarded as a priority for the global health community (Figure 7).

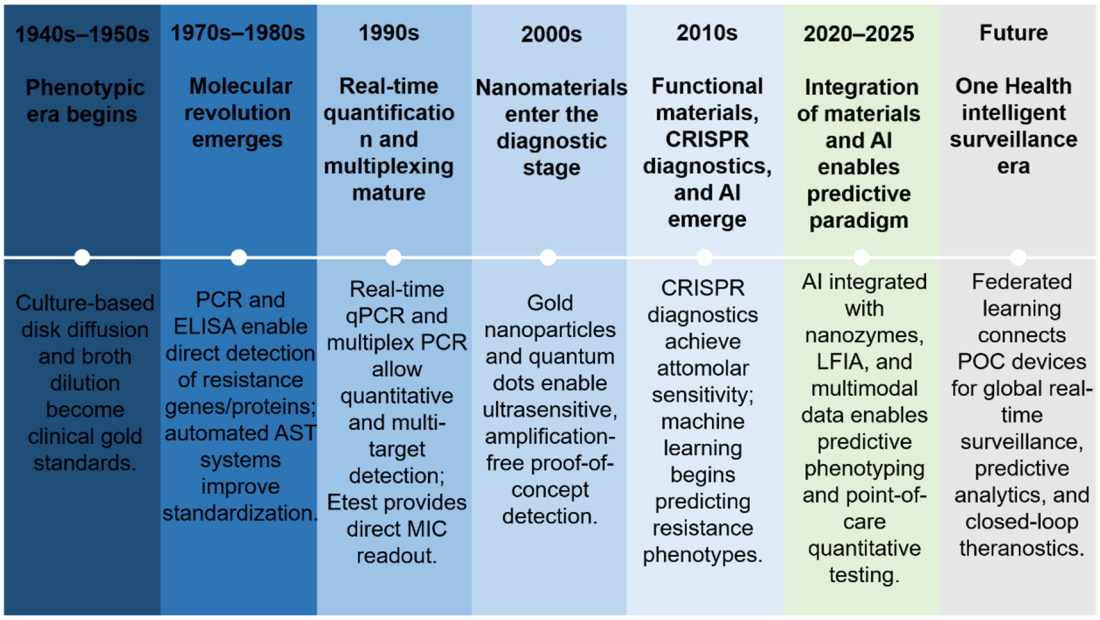

Figure 7. Timeline Evolution of Antimicrobial Resistance Detection Technologies.

6.7. Emerging Frontiers: Wearable Sensors and Closed-Loop Systems

Flexible and stretchable electronic materials, such as conductive polymer hydrogels, have enabled wearable electrochemical sensors for direct integration with chronic wound dressings [191–193]. These sensors continuously monitor pH, uric acid, and impedance, wirelessly transmitting data to a cloud-based AI engine that detects early signs of infection and tracks treatment response. A more transformative prospect lies in converging diagnostic platforms with smart drug delivery systems to create a closed-loop theranostic device. In this conceptual system, an aptamer-functionalized field-effect transistor continuously monitors antibiotic concentrations in interstitial fluid, while a microneedle array delivers the drug from an onboard reservoir in response. The AI controller, receiving real-time pharmacokinetic data, would modulate the delivery rate to maintain the antibiotic concentration within the therapeutic window using a model predictive control algorithm. While this vision remains several years from clinical realization, its component technologies are each advancing rapidly, and their integration represents one of the most exciting long-term prospects of the field.

7. Conclusions

The global dissemination of antimicrobial resistance represents as much a diagnostic crisis as a therapeutic one. The clinical laboratory methods used for resistance detection, while indispensable, are constrained by fundamental limitations that incremental refinement alone cannot fully overcome. Culture-based AST provides the clinically essential minimum inhibitory concentration but imposes a delay that forces empirical prescribing. Molecular techniques compress this timeline yet cannot reveal the functional activity of resistance enzymes, detect unknown mutations, or capture the synergistic interplay of multiple coexisting mechanisms that collectively define the resistance phenotype. Rather than isolated deficiencies, these shortcomings represent three interdependent diagnostic gaps—temporal, mechanistic, and interpretive—that together form the analytical framework of this review and define the design requirements for next-generation AMR diagnostics.

Closing these gaps requires a paradigm shift from static, single-parameter, endpoint assays to dynamic, multi-parametric, and predictive diagnostic platforms. The core proposition of this review is that such platforms can be realized through the deep integration of advanced functional materials and AI. Functional materials serve as the sensing hardware, exploiting their intrinsic nanoscale properties to directly transduce molecular interactions into quantitative signals within minutes rather than days. Through their respective properties—localized surface plasmon resonance in gold nanoparticles, fluorescence quenching in graphene oxide, enzyme-mimetic catalytic cascades in metal-organic frameworks, and real-time impedance sensitivity in microelectrode arrays—these functional materials collectively deliver capabilities long beyond the reach of conventional diagnostics: amplification-free gene detection, direct enzymatic quantification, and dynamic biofilm tolerance monitoring. AI serves as the analytical software, deploying architectures that range from convolutional neural networks for biosensor signal processing to random forests and graph neural networks for multimodal data fusion and rational material design. It is the synergistic coupling of these two domains, materials that generate rich functional data and AI models that decode it, that transforms detection from a passive, descriptive observation into an active, predictive capability.

Translating this conceptual promise into routine clinical practice will be a protracted and complex undertaking. Significant barriers must be overcome, and a clear-eyed assessment of these challenges is essential. Several interconnected obstacles demand sustained interdisciplinary effort: ensuring the batch-to-batch reproducibility of engineered nanomaterials, achieving AI model generalizability across sensor batches and clinical settings, mitigating biofouling in complex biological samples, establishing regulatory frameworks for hybrid hardware-software diagnostics, and securing genuine affordability in the low-resource settings that bear the heaviest AMR burden. These are not problems to be acknowledged only in concluding remarks but design constraints that must be integrated from the earliest stages of technology development.

Notwithstanding these challenges, the trajectory is clear. The 21st-century response to antimicrobial resistance will not be built on new antibiotics alone. It will depend equally on a new generation of diagnostics that are rapid enough to guide initial therapy, mechanistic enough to inform rational antibiotic selection, quantitative enough to predict treatment outcomes, and affordable enough to be deployed wherever they are needed. The fusion of functional materials and AI, as critically examined in this review, provides the foundational science and technology for that vision. Realizing it will require continued innovation, rigorous clinical validation, pragmatic health economic analysis, and a collective commitment to equitable global deployment. While the challenge of antimicrobial resistance remains substantial, the requisite tools are maturing. The imperative now is to translate these advances into equitable clinical and public health impact.

Author Contributions

A.Q. and Y.S. contributed equally to this work. A.Q.: investigation, methodology, writing—original draft; Y.S.: investigation, methodology; C.G.: supervision, funding acquisition; B.C.: conceptualization, writing—review and editing (corresponding author); G.L.: conceptualization, funding acquisition, writing—review and editing (corresponding author). All authors have read and agreed to the published version of the manuscript.

Funding

This work was supported by grants from the National Natural Science Foundation of China (82373637, 82073611) and the Natural Science Foundation of Jiangsu Province (BK20231241, BK20250893).

Institutional Review Board Statement

Not applicable.

Informed Consent Statement

Not applicable.

Data Availability Statement

The data supporting this review article can be obtained from authors or references.

Conflicts of Interest

The authors declare no conflict of interest.

Use of AI and AI-Assisted Technologies

During the preparation of this work, the author used Large Language Models for spelling and grammar checks. After using this tool, the author reviewed and edited the content as needed and takes full responsibility for the content of the published article.

References

1. Davies, J.; Davies, D. Origins and evolution of antibiotic resistance. *Microbiol. Mol. Biol. Rev.* **2010**, *74*, 417–433. https://doi.org/10.1128/mmbr.00016-10.
2. Naghavi, M.; Vollset, S.E.; Ikuta, K.; et al. SGlobal burden of bacterial antimicrobial resistance 1990–2021: A systematic analysis with forecasts to 2050. *Lancet* **2024**, *404*, 1199–1226.
3. Marino, A.; Maniaci, A.; Lentini, M.; et al. The Global Burden of Multidrug-Resistant Bacteria. *Epidemiologia* **2025**, *6*, 21.
4. Daruka, L.; Czikkely, M.S.; Szili, P.; et al. ESKAPE pathogens rapidly develop resistance against antibiotics in development in vitro. *Nat. Microbiol.* **2025**, *10*, 313–331. https://doi.org/10.1038/s41564-024-01891-8.
5. Sati, H.; Carrara, E.; Savoldi, A.; et al. The WHO Bacterial Priority Pathogens List 2024: A prioritisation study to guide research, development, and public health strategies against antimicrobial resistance. *Lancet Infect. Dis.* **2025**, *25*, 1033–1043.
6. Bertagnolio, S.; Dobreva, Z.; Centner, C.M.; et al. WHO global research priorities for antimicrobial resistance in human health. *Lancet Microbe* **2024**, *5*, 100902. https://doi.org/10.1016/s2666-5247(24)00134-4.
7. Okeke, I.N.; de Kraker, M.E.A.; Van Boeckel, T.P.; et al. The scope of the antimicrobial resistance challenge. *Lancet* **2024**, *403*, 2426–2438.
8. Wiegand, I.; Hilpert, K.; Hancock, R.E. Agar and broth dilution methods to determine the minimal inhibitory concentration (MIC) of antimicrobial substances. *Nat. Protoc.* **2008**, *3*, 163–175. https://doi.org/10.1038/nprot.2007.521.
9. Heatley, N.G. A method for the assay of penicillin. *Biochem. J.* **1944**, *38*, 61–65. https://doi.org/10.1042/bj0380061.
10. Nonhoff, C.; Rottiers, S.; Struelens, M.J. Evaluation of the Vitek 2 system for identification and antimicrobial susceptibility testing of *Staphylococcus* spp. *Clin. Microbiol. Infect.* **2005**, *11*, 150–153.
11. Rhoads, S.; Marinelli, L.; Imperatrice, C.A.; et al. Comparison of MicroScan WalkAway system and Vitek system for identification of gram-negative bacteria. *J. Clin. Microbiol.* **1995**, *33*, 3044–3046. https://doi.org/10.1128/jcm.33.11.3044-3046.1995.
12. Hotchkiss, R.S.; Moldawer, L.L.; Opal, S.M.; et al. Sepsis and septic shock. *Nature reviews Disease primers* **2016**, *2*, 16045. https://doi.org/10.1038/nrdp.2016.45.
13. Depka, D.; Mikucka, A.; Bogiel, T.; et al. Conventional and Real-Time PCR Targeting bla(OXA) Genes as Reliable Methods for a Rapid Detection of Carbapenem-Resistant Acinetobacter baumannii Clinical Strains. *Antibiotics* **2022**, *11*, 455.

14. Heid, C.A.; Stevens, J.; Livak, K.J.; et al. Real time quantitative PCR. *Genome Res.* **1996**, *6*, 986–994. https://doi.org/10.1101/gr.6.10.986.
15. Elnifro, E.M.; Ashshi, A.M.; Cooper, R.J.; et al. Multiplex PCR: Optimization and application in diagnostic virology. *Clin. Microbiol. Rev.* **2000**, *13*, 559–570. https://doi.org/10.1128/cmr.13.4.559.
16. Li, C.; Kang, N.; Ye, S.; et al. All-In-One OsciDrop Digital PCR System for Automated and Highly Multiplexed Molecular Diagnostics. *Adv. Sci.* **2024**, *11*, e2309557.
17. Eldin, C.; Parola, P.; Raoult, D. Limitations of diagnostic tests for bacterial infections. *Med. Mal. Infect.* **2019**, *49*, 98–101. https://doi.org/10.1016/j.medmal.2018.12.004.
18. Yee, R.; Dien Bard, J.; Simner, P.J. The Genotype-to-Phenotype Dilemma: How Should Laboratories Approach Discordant Susceptibility Results? *J. Clin. Microbiol.* **2021**, *59*. https://doi.org/10.1128/jcm.00138-20.
19. Analytical Methods Committee. PCR—The polymerase chain reaction. *Anal. Methods* **2014**, *6*, 333–336.
20. Angus, D.C.; van der Poll, T. Severe sepsis and septic shock. *N. Engl. J. Med.* **2013**, *369*, 840–851. https://doi.org/10.1056/nejmra1208623.
21. Burnham, C.D.; Leeds, J.; Nordmann, P.; et al. Diagnosing antimicrobial resistance. *Nat. Rev. Microbiol.* **2017**, *15*, 697–703. https://doi.org/10.1038/nrmicro.2017.103.
22. Vergauwe, F.; De Waele, G.; Sass, A.; et al. Harnessing machine learning to predict antibiotic susceptibility in Pseudomonas aeruginosa biofilms. *NPJ Biofilms Microbiomes* **2025**, *11*, 205. https://doi.org/10.1038/s41522-025-00833-4.
23. Bush, K.; Bradford, P.A. Epidemiology of β-Lactamase-Producing Pathogens. *Clin. Microbiol. Rev.* **2020**, *33*. https://doi.org/10.1128/cmr.00047-19.
24. Queenan, A.M.; Bush, K. Carbapenemases: The versatile beta-lactamases. *Clin. Microbiol. Rev.* **2007**, *20*, 440–458. https://doi.org/10.1128/cmr.00001-07.
25. Bush, K. The ABCD's of β-lactamase nomenclature. *J. Infect. Chemother.* **2013**, *19*, 549–559.
26. Sirot, D.; Sirot, J.; Labia, R.; et al. Transferable resistance to third-generation cephalosporins in clinical isolates of Klebsiella pneumoniae: Identification of CTX-1, a novel beta-lactamase. *J. Antimicrob. Chemother.* **1987**, *20*, 323–334. https://doi.org/10.1093/jac/20.3.323.
27. Walther-Rasmussen, J.; Høiby, N. Class A carbapenemases. *J. Antimicrob. Chemother.* **2007**, *60*, 470–482. https://doi.org/10.1093/jac/dkm226.
28. Chen, L.; Mathema, B.; Chavda, K.D.; et al. Carbapenemase-producing Klebsiella pneumoniae: Molecular and genetic decoding. *Trends Microbiol.* **2014**, *22*, 686–696. https://doi.org/10.1016/j.tim.2014.09.003.
29. Cornaglia, G.; Giamarellou, H.; Rossolini, G.M. Metallo-β-lactamases: A last frontier for β-lactams? *Lancet Infect. Dis.* **2011**, *11*, 381–393. https://doi.org/10.1016/s1473-3099(11)70056-1.
30. Jacoby, G.A. AmpC beta-lactamases. *Clin. Microbiol. Rev.* **2009**, *22*, 161–182. https://doi.org/10.1128/cmr.00036-08.
31. Evans, B.A.; Amyes, S.G. OXA β-lactamases. *Clin. Microbiol. Rev.* **2014**, *27*, 241–263. https://doi.org/10.1128/cmr.00117-13.
32. Park, S.R.; Park, J.W.; Ban, Y.H.; et al. 2-Deoxystreptamine-containing aminoglycoside antibiotics: Recent advances in the characterization and manipulation of their biosynthetic pathways. *Nat. Prod. Rep.* **2013**, *30*, 11–20. https://doi.org/10.1039/c2np20092a.
33. Ramirez, M.S.; Tolmasky, M.E. Aminoglycoside modifying enzymes. *Drug Resist. Updates* **2010**, *13*, 151–171.
34. Azucena, E.; Mobashery, S. Aminoglycoside-modifying enzymes: Mechanisms of catalytic processes and inhibition. *Drug Resist. Updates* **2001**, *4*, 106–117.
35. Shepherd, M.J.; Fu, T.; Harrington, N.E.; et al. Ecological and evolutionary mechanisms driving within-patient emergence of antimicrobial resistance. *Nat. Rev. Microbiol.* **2024**, *22*, 650–665. https://doi.org/10.1038/s41579-024-01041-1.
36. Feng, S.; Wu, Z.; Liang, W.; et al. Prediction of Antibiotic Resistance Evolution by Growth Measurement of All Proximal Mutants of Beta-Lactamase. *Mol. Biol. Evol.* **2022**, *39*, msac086. https://doi.org/10.1093/molbev/msac086.
37. Blair, J.M.; Webber, M.A.; Baylay, A.J.; et al. Molecular mechanisms of antibiotic resistance. *Nat. Rev. Microbiol.* **2015**, *13*, 42–51. https://doi.org/10.1038/nrmicro3380.
38. Wang, Q.; Wei, S.; Silva, A.F.; et al. Cooperative antibiotic resistance facilitates horizontal gene transfer. *ISME J.* **2023**, *17*, 846–854. https://doi.org/10.1038/s41396-023-01393-1.
39. Connell, S.R.; Tracz, D.M.; Nierhaus, K.H.; et al. Ribosomal protection proteins and their mechanism of tetracycline resistance. *Antimicrob. Agents Chemother.* **2003**, *47*, 3675–3681. https://doi.org/10.1128/aac.47.12.3675-3681.2003.
40. Dönhöfer, A.; Franckenberg, S.; Wickles, S.; et al. Structural basis for TetM-mediated tetracycline resistance. *Proc. Natl. Acad. Sci. USA* **2012**, *109*, 16900–16905. https://doi.org/10.1073/pnas.1208037109.
41. Li, W.; Atkinson, G.C.; Thakor, N.S.; et al. Mechanism of tetracycline resistance by ribosomal protection protein Tet(O). *Nat. Commun.* **2013**, *4*, 1477. https://doi.org/10.1038/ncomms2470.
42. Kittl, S.; Brodard, I.; Tresch, M.; et al. Novel tetracycline resistance gene tet(65) located on a multi-resistance Corynebacterium plasmid. *J. Antimicrob. Chemother.* **2024**, *79*, 1023–1029. https://doi.org/10.1093/jac/dkae066.

43. Zhu, Y.; Wang, C.; Schwarz, S.; et al. Identification of a novel tetracycline resistance gene, tet(63), located on a multiresistance plasmid from Staphylococcus aureus. *J. Antimicrob. Chemother.* **2021**, *76*, 576–581. https://doi.org/10.1093/jac/dkaa485.
44. Tomlinson, J.H.; Kalverda, A.P.; Calabrese, A.N. Fusidic acid resistance through changes in the dynamics of the drug target. *Proc. Natl. Acad. Sci. USA* **2020**, *117*, 25523–25531. https://doi.org/10.1073/pnas.2008577117.
45. Leclercq, R.; Courvalin, P. Bacterial resistance to macrolide, lincosamide, and streptogramin antibiotics by target modification. *Antimicrob. Agents Chemother.* **1991**, *35*, 1267–1272. https://doi.org/10.1128/aac.35.7.1267.
46. Martínez-Trejo, A.; Ruiz-Ruiz, J.M.; Gonzalez-Avila, L.U.; et al. Evasion of Antimicrobial Activity in Acinetobacter baumannii by Target Site Modifications: An Effective Resistance Mechanism. *Int. J. Mol. Sci.* **2022**, *23*, 6582. https://doi.org/10.3390/ijms23126582.
47. Lade, H.; Joo, H.S.; Kim, J.S. Molecular Basis of Non-β-Lactam Antibiotics Resistance in Staphylococcus aureus. *Antibiotics* **2022**, *11*, 1378.
48. Lopatkin, A.J.; Bening, S.C.; Manson, A.L.; et al. Clinically relevant mutations in core metabolic genes confer antibiotic resistance. *Science* **2021**, *371*, eaba0862.
49. Campbell, E.A.; Korzheva, N.; Mustaev, A.; et al. Structural mechanism for rifampicin inhibition of bacterial rna polymerase. *Cell* **2001**, *104*, 901–912. https://doi.org/10.1016/s0092-8674(01)00286-0.
50. Blaskovich, M.A.T.; Hansford, K.A.; Butler, M.S.; et al. Developments in Glycopeptide Antibiotics. *ACS Infect. Dis.* **2018**, *4*, 715–735. https://doi.org/10.1021/acsinfecdis.7b00258.
51. Stogios, P.J.; Savchenko, A. Molecular mechanisms of vancomycin resistance. *Protein Sci.* **2020**, *29*, 654–669.
52. Piddock, L.J. Clinically relevant chromosomally encoded multidrug resistance efflux pumps in bacteria. *Clin. Microbiol. Rev.* **2006**, *19*, 382–402. https://doi.org/10.1128/cmr.19.2.382-402.2006.
53. Wong, K.; Ma, J.; Rothnie, A.; et al. Towards understanding promiscuity in multidrug efflux pumps. *Trends Biochem. Sci.* **2014**, *39*, 8–16. https://doi.org/10.1016/j.tibs.2013.11.002.
54. Hirakata, Y.; Srikumar, R.; Poole, K.; et al. Multidrug efflux systems play an important role in the invasiveness of Pseudomonas aeruginosa. *J. Exp. Med.* **2002**, *196*, 109–118. https://doi.org/10.1084/jem.20020005.
55. Pradel, E.; Pagès, J.M. The AcrAB-TolC efflux pump contributes to multidrug resistance in the nosocomial pathogen Enterobacter aerogenes. *Antimicrob. Agents Chemother.* **2002**, *46*, 2640–2643. https://doi.org/10.1128/aac.46.8.2640-2643.2002.
56. Chevalier, S.; Bouffartigues, E.; Bodilis, J.; et al. Structure, function and regulation of Pseudomonas aeruginosa porins. *FEMS Microbiol. Rev.* **2017**, *41*, 698–722. https://doi.org/10.1093/femsre/fux020.
57. Bell, A.; Bains, M.; Hancock, R.E. Pseudomonas aeruginosa outer membrane protein OprH: Expression from the cloned gene and function in EDTA and gentamicin resistance. *J. Bacteriol.* **1991**, *173*, 6657–6664. https://doi.org/10.1128/jb.173.21.6657-6664.1991.
58. Nie, D.; Hu, Y.; Chen, Z.; et al. Outer membrane protein A (OmpA) as a potential therapeutic target for Acinetobacter baumannii infection. *J. Biomed. Sci.* **2020**, *27*, 26. https://doi.org/10.1186/s12929-020-0617-7.
59. Scribano, D.; Cheri, E.; Pompilio, A.; et al. Acinetobacter baumannii OmpA-like porins: Functional characterization of bacterial physiology, antibiotic-resistance, and virulence. *Commun. Biol.* **2024**, *7*, 948. https://doi.org/10.1038/s42003-024-06645-0.
60. Lister, P.D.; Wolter, D.J.; Hanson, N.D. Antibacterial-resistant Pseudomonas aeruginosa: Clinical impact and complex regulation of chromosomally encoded resistance mechanisms. *Clin. Microbiol. Rev.* **2009**, *22*, 582–610. https://doi.org/10.1128/cmr.00040-09.
61. Roemhild, R.; Bollenbach, T.; Andersson, D.I. The physiology and genetics of bacterial responses to antibiotic combinations. *Nat. Rev. Microbiol.* **2022**, *20*, 478–490. https://doi.org/10.1038/s41579-022-00700-5.
62. O'Toole, G.; Kaplan, H.B.; Kolter, R. Biofilm formation as microbial development. *Annu. Rev. Microbiol.* **2000**, *54*, 49–79. https://doi.org/10.1146/annurev.micro.54.1.49.
63. Hall, C.W.; Mah, T.F. Molecular mechanisms of biofilm-based antibiotic resistance and tolerance in pathogenic bacteria. *FEMS Microbiol. Rev.* **2017**, *41*, 276–301. https://doi.org/10.1093/femsre/fux010.
64. Taylor, P.K.; Yeung, A.T.; Hancock, R.E. Antibiotic resistance in Pseudomonas aeruginosa biofilms: Towards the development of novel anti-biofilm therapies. *J. Biotechnol.* **2014**, *191*, 121–130. https://doi.org/10.1016/j.jbiotec.2014.09.003.
65. Harms, A.; Maisonneuve, E.; Gerdes, K. Mechanisms of bacterial persistence during stress and antibiotic exposure. *Science* **2016**, *354*, aaf4268.
66. Rossi, E.; La Rosa, R.; Bartell, J.A.; et al. Pseudomonas aeruginosa adaptation and evolution in patients with cystic fibrosis. *Nat. Rev. Microbiol.* **2021**, *19*, 331–342. https://doi.org/10.1038/s41579-020-00477-5.
67. Bassetti, M.; Poulakou, G.; Ruppe, E.; et al. Antimicrobial resistance in the next 30 years, humankind, bugs and drugs: A visionary approach. *Intensive Care Med.* **2017**, *43*, 1464–1475. https://doi.org/10.1007/s00134-017-4878-x.
68. Dina, N.E.; Tahir, M.A.; Bajwa, S.Z.; et al. SERS-based antibiotic susceptibility testing: Towards point-of-care clinical diagnosis. *Biosens. Bioelectron.* **2023**, *219*, 114843. https://doi.org/10.1016/j.bios.2022.114843.

69. Jorgensen, J.H.; Ferraro, M.J. Antimicrobial susceptibility testing: A review of general principles and contemporary practices. *Clin. Infect. Dis.* **2009**, *49*, 1749–1755.
70. Belanger, C.R.; Hancock, R.E.W. Testing physiologically relevant conditions in minimal inhibitory concentration assays. *Nat. Protoc.* **2021**, *16*, 3761–3774. https://doi.org/10.1038/s41596-021-00572-8.
71. Berkow, E.L.; Lockhart, S.R.; Ostrosky-Zeichner, L. Antifungal Susceptibility Testing: Current Approaches. *Clin. Microbiol. Rev.* **2020**, *33*. https://doi.org/10.1128/cmr.00069-19.
72. Baquer, F.; Ali Sawan, A.; Auzou, M.; et al. Broth Microdilution and Gradient Diffusion Strips vs. Reference Agar Dilution Method: First Evaluation for Clostridiales Species Antimicrobial Susceptibility Testing. *Antibiotics* **2021**, *10*, 975.
73. Hanson, C.W.; Martin, W.J. Modified agar dilution method for rapid antibiotic susceptibility testing of anaerobic bacteria. *Antimicrob. Agents Chemother.* **1978**, *13*, 383–388. https://doi.org/10.1128/aac.13.3.383.
74. Brook, I.; Wexler, H.M.; Goldstein, E.J. Antianaerobic antimicrobials: Spectrum and susceptibility testing. *Clin. Microbiol. Rev.* **2013**, *26*, 526–546. https://doi.org/10.1128/cmr.00086-12.
75. Nijs, A.; Cartuyvels, R.; Mewis, A.; et al. Comparison and evaluation of Osiris and Sirscan 2000 antimicrobial susceptibility systems in the clinical microbiology laboratory. *J. Clin. Microbiol.* **2003**, *41*, 3627–3630. https://doi.org/10.1128/jcm.41.8.3627-3630.2003.
76. Kustimur, S.; Kalkanci, A.; Mansuroglu, H.; et al. Evaluation of the disc diffusion method with a comparison study for fluconazole susceptibility of Candida strains. *Chin. Med. J.* **2003**, *116*, 633–636.
77. Citron, D.M.; Ostovari, M.I.; Karlsson, A.; et al. Evaluation of the E test for susceptibility testing of anaerobic bacteria. *J. Clin. Microbiol.* **1991**, *29*, 2197–2203. https://doi.org/10.1128/jcm.29.10.2197-2203.1991.
78. Jönsson, A.; Jacobsson, S.; Foerster, S.; et al. Performance characteristics of newer MIC gradient strip tests compared with the Etest for antimicrobial susceptibility testing of Neisseria gonorrhoeae. *Apmis* **2018**, *126*, 822–827.
79. Huang, M.B.; Baker, C.N.; Banerjee, S.; et al. Accuracy of the E test for determining antimicrobial susceptibilities of staphylococci, enterococci, *Campylobacter jejuni*, and gram-negative bacteria resistant to antimicrobial agents. *J. Clin. Microbiol.* **1992**, *30*, 3243–3248. https://doi.org/10.1128/jcm.30.12.3243-3248.1992.
80. Jorgensen, J.H.; Ferraro, M.J.; McElmeel, M.L.; et al. Detection of penicillin and extended-spectrum cephalosporin resistance among Streptococcus pneumoniae clinical isolates by use of the E test. *J. Clin. Microbiol.* **1994**, *32*, 159–163. https://doi.org/10.1128/jcm.32.1.159-163.1994.
81. O'Hara, C.M. Manual and automated instrumentation for identification of Enterobacteriaceae and other aerobic gram-negative bacilli. *Clin. Microbiol. Rev.* **2005**, *18*, 147–162.
82. Rodríguez, L.A.; Vivas, J.; Gallardo, C.S.; et al. Identification of Hafnia alvei with the MicroScan WalkAway system. *J. Clin. Microbiol.* **1999**, *37*, 4186–4188. https://doi.org/10.1128/jcm.37.12.4186-4188.1999.
83. Steward, C.D.; Mohammed, J.M.; Swenson, J.M.; et al. Antimicrobial susceptibility testing of carbapenems: Multicenter validity testing and accuracy levels of five antimicrobial test methods for detecting resistance in Enterobacteriaceae and Pseudomonas aeruginosa isolates. *J. Clin. Microbiol.* **2003**, *41*, 351–358. https://doi.org/10.1128/jcm.41.1.351-358.2003.
84. Zhou, X.; Dai, Y.Y.; Ma, X.L. Be alert to the alterations in the biological characteristics in heterogeneous vancomycin-intermediate Staphylococcus aureus. *Indian J. Med. Microbiol.* **2012**, *30*, 215–217. https://doi.org/10.4103/0255-0857.96696.
85. Renders, N.H.; Kluytmans, J.A.; Verbrugh, H.A. Clinical impact of rapid in vitro susceptibility testing and bacterial identification. *J. Clin. Microbiol.* **1995**, *33*, 508. https://doi.org/10.1128/jcm.33.2.508-508.1995.
86. Llor, C.; Bjerrum, L. Antimicrobial resistance: Risk associated with antibiotic overuse and initiatives to reduce the problem. *Ther. Adv. Drug Saf.* **2014**, *5*, 229–241. https://doi.org/10.1177/2042098614554919.
87. Zafar, A.; Khursheed, N.; Adnan, F.; et al. Determination of Inducible Clindamycin Resistance and Correlation with Vitek2 Inducible Clindamycin Resistance Test in *Staphylococcus aureus* Isolated from Clinical Samples. *J. Coll. Physicians Surg.* **2024**, *34*, 183–186. https://doi.org/10.29271/jcpsp.2024.02.183.
88. Tsakris, A.; Poulou, A.; Bogaerts, P.; et al. Evaluation of a new phenotypic OXA-48 disk test for differentiation of OXA-48 carbapenemase-producing Enterobacteriaceae clinical isolates. *J. Clin. Microbiol.* **2015**, *53*, 1245–1251. https://doi.org/10.1128/jcm.03318-14.
89. Itahashi, M.; Higaki, S.; Fukuda, M.; et al. Detection and quantification of pathogenic bacteria and fungi using real-time polymerase chain reaction by cycling probe in patients with corneal ulcer. *Arch. Ophthalmol.* **2010**, *128*, 535–540.
90. Kurkela, S.; Brown, D.W.G. Molecular diagnostic techniques. *Medicine* **2009**, *37*, 535–540.
91. Yang, B.; Xin, X.; Cao, X.; et al. Phenotypic and genotypic perspectives on detection methods for bacterial antimicrobial resistance in a One Health context: Research progress and prospects. *Arch. Microbiol.* **2024**, *206*, 409. https://doi.org/10.1007/s00203-024-04131-z.
92. Abd El-Aziz, N.; Abd El-Hamid, M.; Bendary, M.; et al. Existence of vancomycin resistance among methicillin resistant s. aureus recovered from animal and human sources in Egypt. *Slov. Vet. Res.* **2018**, *55*, 221–230.

93. Pulido, M.R.; García-Quintanilla, M.; Martín-Peña, R.; et al. Progress on the development of rapid methods for antimicrobial susceptibility testing. *J. Antimicrob. Chemother.* **2013**, *68*, 2710–2717. https://doi.org/10.1093/jac/dkt253.
94. Lupo, A.; Papp-Wallace, K.M.; Sendi, P.; et al. Non-phenotypic tests to detect and characterize antibiotic resistance mechanisms in Enterobacteriaceae. *Diagn. Microbiol. Infect. Dis.* **2013**, *77*, 179–194. https://doi.org/10.1016/j.diagmicrobio.2013.06.001.
95. Kim, K.J.; Yun, S.G.; Cho, Y.; et al. Rapid Direct Identification of Microbial Pathogens and Antimicrobial Resistance Genes in Positive Blood Cultures Using a Fully Automated Multiplex PCR Assay. *J. Korean Med. Sci.* **2024**, *39*, e157. https://doi.org/10.3346/jkms.2024.39.e157.
96. Mirabile, A.; Sangiorgio, G.; Bonacci, P.G.; et al. Advancing Pathogen Identification: The Role of Digital PCR in Enhancing Diagnostic Power in Different Settings. *Diagnostics* **2024**, *14*, 1598.
97. Zhu, J.; Liu, B.; Shu, X.; et al. A novel mutation of walK confers vancomycin-intermediate resistance in methicillin-susceptible Staphylococcus aureus. *Int. J. Med. Microbiol.* **2021**, *311*, 151473. https://doi.org/10.1016/j.ijmm.2021.151473.
98. Ruiying, F.; Lianchao, W.; Xutian, Y.; et al. Defects-Engineered Metal-Organic Frameworks for Supercapacitor Platform. *Sustain. Eng. Novit* **2025**, *1*, 2.
99. Gn, Y.; Yn, C.; Wn, R.; et al. Hybrid and Flow-Electrode Capacitive Deionization: Materials Design, Multispecies Removal, and Smart Regulation. *Sustain. Eng. Novit* **2025**, *1*, 7.
100. Hang, Y.; Wang, A.; Wu, N. Plasmonic silver and gold nanoparticles: Shape- and structure-modulated plasmonic functionality for point-of-caring sensing, bio-imaging and medical therapy. *Chem. Soc. Rev.* **2024**, *53*, 2932–2971. https://doi.org/10.1039/d3cs00793f.
101. Palani, S.; Kenison, J.P.; Sabuncu, S.; et al. Multispectral Localized Surface Plasmon Resonance (msLSPR) Reveals and Overcomes Spectral and Sensing Heterogeneities of Single Gold Nanoparticles. *ACS Nano* **2023**, *17*, 2266–2278.
102. Mayaka, R.K.; Alocilja, E.C. Genomic nano-biosensor for rapid detection of the carbapenem-resistant gene bla (NDM-1) in carbapenemase-producing bacteria. *Nanoscale Adv.* **2025**, *7*, 2518–2527. https://doi.org/10.1039/d4na00798k.
103. Kao, K.; Alocilja, E.C. Integrated Sample to Detection of Carbapenem-Resistant Bacteria Extracted from Water Samples Using a Portable Gold Nanoparticle-Based Biosensor. *Sensors* **2025**, *25*, 5293.
104. Kao, K.; Alocilja, E.C. Parallel Detection of the Unamplified Carbapenem Resistance Genes bla(NDM-1) and bla(OXA-1) Using a Plasmonic Nano-Biosensor with a Field-Portable DNA Extraction Method. *Biosensors* **2025**, *15*, 112. https://doi.org/10.3390/bios15020112.
105. Wu, J.; Lin, H.; Moss, D.J.; et al. Graphene oxide for photonics, electronics and optoelectronics. *Nat. Rev. Chem.* **2023**, *7*, 162–183. https://doi.org/10.1038/s41570-022-00458-7.
106. Gao, L.; Lian, C.; Zhou, Y.; et al. Graphene oxide–DNA based sensors. *Biosens. Bioelectron.* **2014**, *60*, 22–29. https://doi.org/10.1016/j.bios.2014.03.039.
107. Wang, P.; Dimitrijevic, N.M.; Chang, A.Y.; et al. Photoinduced electron transfer pathways in hydrogen-evolving reduced graphene oxide-boosted hybrid nano-bio catalyst. *ACS Nano* **2014**, *8*, 7995–8002.
108. Xiao, X.; Zhang, Y.; Zhou, L.; et al. Photoluminescence and Fluorescence Quenching of Graphene Oxide: A Review. *Nanomaterials* **2022**, *12*, 2444.
109. Kang, J.; Nguyen, V.T.; Kim, M.S. Rapid and Sensitive Detection of Antibiotic Resistance Genes by Utilizing TALEs as a Diagnostic Probe with 2D-Nanosheet Graphene Oxide. *Anal. Chem.* **2023**, *95*, 9505–9512. https://doi.org/10.1021/acs.analchem.3c00647.
110. Biesold, G.M.; Liang, S.; Brettmann, B.; et al. Tailoring Optical Properties of Luminescent Semiconducting Nanocrystals through Hydrostatic, Anisotropic Static, and Dynamic Pressures. *Angew. Chem. Int. Ed.* **2021**, *60*, 9772–9788. https://doi.org/10.1002/anie.202008395.
111. Lu, H.; Li, W.; Dong, H.; et al. Graphene Quantum Dots for Optical Bioimaging. *Small* **2019**, *15*, e1902136.
112. Hu, O.; Li, Z.; He, Q.; et al. Fluorescence Biosensor for One-Step Simultaneous Detection of Mycobacterium tuberculosis Multidrug-Resistant Genes Using nanoCoTPyP and Double Quantum Dots. *Anal. Chem.* **2022**, *94*, 7918–7927. https://doi.org/10.1021/acs.analchem.2c00723.
113. Medintz, I.L.; Uyeda, H.T.; Goldman, E.R.; et al. Quantum dot bioconjugates for imaging, labelling and sensing. *Nat. Mater.* **2005**, *4*, 435–446. https://doi.org/10.1038/nmat1390.
114. Escamilla, P.; Bartella, L.; Sanz-Navarro, S.; et al. Degradation of Penicillinic Antibiotics and β-Lactamase Enzymatic Catalysis in a Biomimetic Zn-Based Metal-Organic Framework. *Chemistry* **2023**, *29*, e202301325.
115. Huo, Y.P.; Liu, S.; Gao, Z.X.; et al. State-of-the-art progress of switch fluorescence biosensors based on metal-organic frameworks and nucleic acids. *Mikrochim. Acta* **2021**, *188*, 168. https://doi.org/10.1007/s00604-021-04827-9.
116. Yao, J.; Lu, Y.; Sun, H.; et al. Engineering for Covalent Organic Framework Membranes. *Chem. Res. Chin. Univ.* **2022**, *38*, 364–372. https://doi.org/10.1007/s40242-022-1507-1.
117. Ma, J.; Lu, X.; Liu, S.; et al. Fabrication of fluorescence sensor array for discrimination subtypes of aminoglycosides leveraging MOF-based inhibition reactions and thiol-response metal nanoclusters. *Biosens. Bioelectron.* **2025**, *287*, 117652. https://doi.org/10.1016/j.bios.2025.117652.

118. Yang, L.; Fu, Z.; Xie, J.; et al. Portable sensing of hydrogen peroxide using MOF-based nanozymes. *Food Res. Int.* **2024**, *197*, 115272. https://doi.org/10.1016/j.foodres.2024.115272.
119. Li, R.; Qian, G.; Shen, H.; et al. MOF@MOF nanozyme for ultrasensitive and low-background detection of multidrug-resistant bacteria. *Microchem. J.* **2025**, *209*, 112695. https://doi.org/10.1016/j.microc.2025.112695.
120. Li, R.; Fan, H.; Shen, H.; et al. Versatile MOF@COF catalyzed and magnetically multivalent aptamer assisted biosensing platform for rapid and ultrasensitive dual-mode detection of multidrug-resistant bacteria. *Sens. Actuators B Chem.* **2024**, *410*, 135719. https://doi.org/10.1016/j.snb.2024.135719.
121. Chi, H.; Xiao, Y.; Ning, H.; et al. Thiol-ene click reaction aptamer sensor based on MWCNT-COOH/MOF-818 composite for highly sensitive detection of foodborne pathogenic bacteria. *Curr. Res. Food Sci.* **2025**, *11*, 101193. https://doi.org/10.1016/j.crfs.2025.101193.
122. Wang, C.; Luo, Y.; Liu, X.; et al. The enhanced photocatalytic sterilization of MOF-Based nanohybrid for rapid and portable therapy of bacteria-infected open wounds. *Bioact. Mater.* **2022**, *13*, 200–211. https://doi.org/10.1016/j.bioactmat.2021.10.033.
123. Wang, M.; Xiao, C.; Zhao, F.; et al. A label-free electrochemical sensor based on π-structured bipedal DNA walker-triggered hybridization chain reaction and AuPt NPs/Zr-MOF for OTA detection. *Anal. Chim. Acta* **2025**, *1334*, 343424. https://doi.org/10.1016/j.aca.2024.343424.
124. Gao, Z.; Cheng, Y.; Long, C.; et al. Dual-Nanozyme Cascade for System-Wide Specific Colorimetric Detection of Aminoglycoside Antibiotics. *Anal. Chem.* **2025**, *97*, 6136–6144. https://doi.org/10.1021/acs.analchem.4c06854.
125. Nordmann, P.; Helsens, N.; Kieffer, N.; et al. Rapid detection of β-lactamase activity using the rapid Amp NP test. *Microbiol. Spectr.* **2025**, *13*, e0078224. https://doi.org/10.1128/spectrum.00782-24.
126. Yang, C.; Wang, Q.; Ding, W. Recent progress in the imaging detection of enzyme activities in vivo. *RSC Adv.* **2019**, *9*, 25285–25302. https://doi.org/10.1039/c9ra04508b.
127. Chen, F.; Li, Y.; Peng, Y.; et al. Highly Sensitive In Vivo Imaging of Bacterial Infections with a Hydrophilicity-Switching, Self-Immobilizing, Near-Infrared Fluorogenic β-Lactamase Probe Enriched within Bacteria. *Adv. Sci.* **2025**, *12*, 2408559. https://doi.org/10.1002/advs.202408559.
128. Kong, Y.; Yao, H.; Ren, H.; et al. Imaging tuberculosis with endogenous β-lactamase reporter enzyme fluorescence in live mice. *Proc. Natl. Acad. Sci. USA* **2010**, *107*, 12239–12244. https://doi.org/10.1073/pnas.1000643107.
129. Heuker M. Bacteria-Targeted Infection Imaging. Ph.D. Thesis, University of Groningen, Groningen, The Netherlands, 2021.
130. Yao, Y.; Zhang, Y.; Yan, C.; et al. Enzyme-activatable fluorescent probes for β-galactosidase: From design to biological applications. *Chem. Sci.* **2021**, *12*, 9885–9894. https://doi.org/10.1039/d1sc02069b.
131. Wang, R.; Chen, J.; Gao, J.; et al. A molecular design strategy toward enzyme-activated probes with near-infrared I and II fluorescence for targeted cancer imaging. *Chem. Sci.* **2019**, *10*, 7222–7227. https://doi.org/10.1039/c9sc02093d.
132. Yang, H.J.; Kong, Y.; Cheng, Y.; et al. Real-time Imaging of Mycobacterium tuberculosis, Using a Novel Near-Infrared Fluorescent Substrate. *J. Infect. Dis.* **2017**, *215*, 405–414.
133. Nooshabadi, F.; Yang, H.J.; Cheng, Y.; et al. Intravital excitation increases detection sensitivity for pulmonary tuberculosis by whole-body imaging with β-lactamase reporter enzyme fluorescence. *J. Biophotonics* **2017**, *10*, 821–829. https://doi.org/10.1002/jbio.201600132.
134. Xin, E.Y.H.; Kwek, G.; An, X.; et al. Enzymes in Synergy: Bacteria Specific Molecular Probe for Locoregional Imaging of Urinary Tract Infection in vivo. *Angew. Chem.* **2024**, *63*, e202406843.
135. Zieliński, W.; Grabowska, I. Electrochemical biosensors as emerging alternatives to conventional detection of pathogens and antibiotic-resistance determinants. *Talanta* **2026**, *301*, 129323. https://doi.org/10.1016/j.talanta.2025.129323.
136. Gunasekaran, D.; Rostovsky, I.; Taussig, D.; et al. A dual-channel electrochemical biosensor enables concurrent detection of pathogens and antibiotic resistance. *Biosens. Bioelectron.* **2024**, *257*, 116314. https://doi.org/10.1016/j.bios.2024.116314.
137. Dutta, A.; Mukherjee, S.; Haldar, J.; et al. Augmenting Antimicrobial Resistance Surveillance: Rapid Detection of β-Lactamase-Expressing Drug-Resistant Bacteria through Sensitized Luminescence on a Paper-Supported Hydrogel. *ACS Sens.* **2024**, *9*, 351–360. https://doi.org/10.1021/acssensors.3c02065.
138. Shukla, M.; Maiya, D.; Malaviya, R.; et al. Electrochemical β-lactamase immunostrip sensor with 3D hydrogel-paper scaffold for rapid detection & post-antibiotic therapy monitoring in drug-resistant bloodstream infections. *Anal. Chim. Acta* **2025**, *1353*, 343953. https://doi.org/10.1016/j.aca.2025.343953.
139. Cui, H.S.; Wu, Z.R.; Shi, X.Y.; et al. CS/PVP Hydrogel-Based Nanocapillary for Monitoring Bacterial Growth and Rapid Antibiotic Susceptibility Testing. *ACS Sens.* **2024**, *9*, 3540–3548. https://doi.org/10.1021/acssensors.4c00381.
140. Bottari, F.; Blust, R.; De Wael, K. Bio(inspired) strategies for the electro-sensing of β-lactam antibiotics. *Curr. Opin. Electrochem.* **2018**, *10*, 136–142. https://doi.org/10.1016/j.coelec.2018.05.015.
141. Jamali, S.S.; Somerville, S.V.; Dief, E.M.; et al. Stochastic Electrochemical Measurement of a Biofouling Layer on Gold. *Anal. Chem.* **2024**, *96*, 7401–7410. https://doi.org/10.1021/acs.analchem.3c04868.
142. Shan, S.; Lai, W.; Xiong, Y.; et al. Novel strategies to enhance lateral flow immunoassay sensitivity for detecting foodborne pathogens. *J. Agric. Food Chem.* **2015**, *63*, 745–753. https://doi.org/10.1021/jf5046415.

143. Wang, Y.; Deng, C.; Qian, S.; et al. An ultrasensitive lateral flow immunoassay platform for foodborne biotoxins and pathogenic bacteria based on carbon-dots embedded mesoporous silicon nanoparticles fluorescent reporter probes. *Food Chem.* **2023**, *399*, 133970. https://doi.org/10.1016/j.foodchem.2022.133970.
144. Tong, H.; Cao, C.; You, M.; et al. Artificial intelligence-assisted colorimetric lateral flow immunoassay for sensitive and quantitative detection of COVID-19 neutralizing antibody. *Biosens. Bioelectron.* **2022**, *213*, 114449. https://doi.org/10.1016/j.bios.2022.114449.
145. Sulfianti, A.; Sopandi, V.T.; Isnaeni, I.; et al. Antibody-labelled gold nanoparticles synthesized by laser ablation to detect SARS-CoV-2 antigen spike. *Admet Dmpk* **2024**, *12*, 193–208.
146. Kepceoğlu, A.; Gündoğdu, Y.; Sarilmaz, A.; et al. Rhenium/rhenium oxide nanoparticles production using femtosecond pulsed laser ablation in liquid. *Turk. J. Chem.* **2021**, *45*, 485–492. https://doi.org/10.3906/kim-2008-59.
147. Bielskė, K.; Simanavičius, M.; Nuttens, J.; et al. Novel monoclonal antibodies for immunodetection of AmpC β-lactamases. *PeerJ* **2025**, *13*, e20036. https://doi.org/10.7717/peerj.20036.
148. Moguet, C.; Gonzalez, C.; Naas, T.; et al. Multiplex Lateral Flow Immunoassay for the Detection of Expanded-Spectrum Hydrolysis and CTX-M Enzymes. *Diagnostics* **2022**, *12*, 190.
149. Mancini, S.; Garcia-Verellen, L.; Seth-Smith, H.M.B.; et al. Diagnostic algorithm for the detection of carbapenemases and extended-spectrum β-lactamases in carbapenem-resistant Pseudomonas aeruginosa. *Microbiol. Spectr.* **2025**, *13*, e0319624. https://doi.org/10.1128/spectrum.03196-24.
150. Herrera, A.; Zhou, J.; Song, M.S.; et al. Evolution of Cell-Type-Specific RNA Aptamers via Live Cell-Based SELEX. *Methods Mol. Biol.* **2023**, *2666*, 317–346.
151. Gauger, M.; Duchardt-Ferner, E.; Halbritter, A.J.; et al. Investigating the Conformational Diversity of the TMR-3 Aptamer. *J. Am. Chem. Soc.* **2025**, *147*, 17497–17509. https://doi.org/10.1021/jacs.5c04576.
152. Liu, R.; Yang, Z.; Guo, Q.; et al. Signaling-Probe Displacement Electrochemical Aptamer-based Sensor (SD-EAB) for Detection of Nanomolar Kanamycin A. *Electrochim. Acta* **2015**, *182*, 516–523. https://doi.org/10.1016/j.electacta.2015.09.140.
153. Bao, Y.; Ding, G.; Li, Y.; et al. Signal-On, and Modification-Free Electrochemical Sensing Platform Based on Aptamer Switch Hydrogel. *Anal. Chem.* **2025**, *97*, 23331–23338. https://doi.org/10.1021/acs.analchem.5c04124.
154. Cui, J.; Zhang, Y.; Lun, K.; et al. Sensitive detection of Escherichia coli in diverse foodstuffs by electrochemical aptasensor based on 2D porphyrin-based COF. *Mikrochim. Acta* **2023**, *190*, 421. https://doi.org/10.1007/s00604-023-05978-7.
155. Zhang, J.; Zhu, M.; Yan, H.; et al. Split CRISPR/Cas systems: Pioneering solutions for molecular diagnostics challenges. *Biosens. Bioelectron.* **2026**, *293*, 118177. https://doi.org/10.1016/j.bios.2025.118177.
156. Garneau, J.E.; Dupuis, M.; Villion, M.; et al. The CRISPR/Cas bacterial immune system cleaves bacteriophage and plasmid DNA. *Nature* **2010**, *468*, 67–71. https://doi.org/10.1038/nature09523.
157. Li, X.; Zhang, Y.; He, M.; et al. An ultrasensitive and specific fluorescence split-aptasensor for D-VP detection based on target-induced self-propelled 3D DNA walkers coupled with CRISPR-Cas12a. *Talanta* **2025**, *293*, 128102. https://doi.org/10.1016/j.talanta.2025.128102.
158. Huang, D.; He, Y.; Xu, C.; et al. DNAzyme-Triggered Equilibrium Transfer with Self-Activated CRISPR-Cas12a Biosensor Enables One-Pot Diagnosis of Nucleic Acids. *Anal. Chem.* **2025**, *97*, 3026–3035. https://doi.org/10.1021/acs.analchem.4c06066.
159. Dziuba, A.; Dzierżak, S.; Sodo, A.; et al. Comparative study of virulence potential, phylogenetic origin, CRISPR-Cas regions and drug resistance of Escherichia coli isolates from urine and other clinical materials. *Front. Microbiol.* **2023**, *14*, 1289683. https://doi.org/10.3389/fmicb.2023.1289683.
160. Shu, Y.; Liu, S.; Liu, J. Combining aptamers for thiamphenicol and chloramphenicol for detecting both antibiotics. *Chem. Commun.* **2025**, *61*, 18132–18135.
161. Mason, H.G.; Hu, C.H.; Cordova, L.S.; et al. Rapid Prototyping of Microfluidic Devices with Stereolithographic 3D Printing. *bioRxiv* **2025**, https://doi.org/10.1101/2025.07.10.662041.
162. Tang, P.C.; Eriksson, O.; Sjögren, J.; et al. A Microfluidic Chip for Studies of the Dynamics of Antibiotic Resistance Selection in Bacterial Biofilms. *Front. Cell. Infect. Microbiol.* **2022**, *12*, 896149. https://doi.org/10.3389/fcimb.2022.896149.
163. Tran, V.N.; Khan, F.; Han, W.; et al. Real-time monitoring of mono- and dual-species biofilm formation and eradication using microfluidic platform. *Sci. Rep.* **2022**, *12*, 9678. https://doi.org/10.1038/s41598-022-13699-9.
164. Guliy, O.I.; Evstigneeva, S.S.; Bunin, V.D. Microfluidic bioanalytical system for biofilm formation indication. *Talanta* **2022**, *247*, 123541. https://doi.org/10.1016/j.talanta.2022.123541.
165. Liu, Z.; Qin, S.; Chen, X.; et al. PDMS-PDMS Micro Channels Filled with Phase-Change Material for Chip Cooling. *Micromachines* **2018**, *9*, 165. https://doi.org/10.3390/mi9040165.
166. Pholwat, S.; Liu, J.; Stroup, S.; et al. Integrated microfluidic card with TaqMan probes and high-resolution melt analysis to detect tuberculosis drug resistance mutations across 10 genes. *mBio* **2015**, *6*, e02273. https://doi.org/10.1128/mbio.02273-14.

167. Kulshrestha, A.; Gupta, P.; Negi, S.S. Sustainable and optimized fabrication of microfluidic devices for electrochemical detection and monitoring of microbial biofilms. *Microfluid. Nanofluidics* **2025**, *29*, 34. https://doi.org/10.1007/s10404-025-02804-9.
168. Wang, H.; Yin, Y.; Zhu, Z.J. Encoding LC-MS-Based Untargeted Metabolomics Data into Images toward AI-Based Clinical Diagnosis. *Anal. Chem.* **2023**, *95*, 6533–6541. https://doi.org/10.1021/acs.analchem.2c05079.
169. Liang, S.; Ma, J.; Wang, G.; et al. The Application of Artificial Intelligence in the Diagnosis and Drug Resistance Prediction of Pulmonary Tuberculosis. *Front. Med.* **2022**, *9*, 935080. https://doi.org/10.3389/fmed.2022.935080.
170. Nguyen, H.A.; Peleg, A.Y.; Song, J.; et al. Predicting Pseudomonas aeruginosa drug resistance using artificial intelligence and clinical MALDI-TOF mass spectra. *mSystems* **2024**, *9*, e0078924.
171. Li, Y.; Wang, J.; Pan, X.; et al. MRI-mediated intelligent multimodal imaging system: From artificial intelligence to clinical imaging diagnosis. *Drug Discov. Today* **2025**, *30*, 104399. https://doi.org/10.1016/j.drudis.2025.104399.
172. Batisti Biffignandi, G.; Chindelevitch, L.; Corbella, M.; et al. Optimising machine learning prediction of minimum inhibitory concentrations in Klebsiella pneumoniae. *Microb. Genom.* **2024**, *10*, 001222.
173. Ozcan, A.; Coudert, F.X.; Rogge, S.M.J.; et al. Artificial Intelligence Paradigms for Next-Generation Metal-Organic Framework Research. *J. Am. Chem. Soc.* **2025**, *147*, 23367–23380. https://doi.org/10.1021/jacs.5c08214.
174. Jiang, Z.; Feng, J.; Wang, F.; et al. AI-Guided Design of Antimicrobial Peptide Hydrogels for Precise Treatment of Drug-resistant Bacterial Infections. *Adv. Mater.* **2025**, *37*, e2500043.
175. Wulfert, L.; Kuhnel, J.; Krupp, L.; et al. AIfES: A Next-Generation Edge AI Framework. *IEEE Trans. Pattern Anal. Mach. Intell.* **2024**, *46*, 4519–4533. https://doi.org/10.1109/tpami.2024.3355495.
176. Davis, A.M.; Tomitaka, A. Machine Learning-Based Quantification of Lateral Flow Assay Using Smartphone-Captured Images. *Biosensors* **2025**, *15*, 19. https://doi.org/10.3390/bios15010019.
177. Zhang, Y.; Zhang, L.; Zhang, Z.; et al. Explainable AI multiomics analysis reveals shared and divergent host responses in COVID-19 and influenza. *NPJ Digit. Med.* **2026**, *9*, 111. https://doi.org/10.1038/s41746-025-02291-w.
178. Tian, T.; Zhang, X.; Zhang, F.; et al. Harnessing AI for advancing pathogenic microbiology: A bibliometric and topic modeling approach. *Front. Microbiol.* **2024**, *15*, 1510139. https://doi.org/10.3389/fmicb.2024.1510139.
179. Ong Ly, C.; Unnikrishnan, B.; Tadic, T.; et al. Shortcut learning in medical AI hinders generalization: Method for estimating AI model generalization without external data. *NPJ Digit. Med.* **2024**, *7*, 124.
180. Ryan, K.; Kasun, M.; Roberts, L.W., et al. Information, collaboration, regulation: Physician and AI researcher views on ethical considerations in clinical AI integration. *Big Data Soc.* **2025**, *12*, 20539517251343853.
181. Yang, M.; Shi, Y.; Wang, F.; et al. Hydrogel Microspheres as Versatile Platforms for Biomedical Research: Design, Properties, and Applications. *MedComm* **2025**, *6*, e70423. https://doi.org/10.1002/mco2.70423.
182. Ma, C.; Zhang, H.; Rao, Y.; et al. AI-driven virtual cell models in preclinical research: Technical pathways, validation mechanisms, and clinical translation potential. *NPJ Digit. Med.* **2025**, *9*, 25. https://doi.org/10.1038/s41746-025-02198-6.
183. Wang, T.; Su, E. Guardians of Future Food Safety: Innovative Applications and Advancements in Anti-biofouling Materials. *J. Agric. Food Chem.* **2024**, *72*, 21973–21985. https://doi.org/10.1021/acs.jafc.4c05156.
184. Alazzam, I.; Ait-Mouheb, N.; Knapp, Y.; et al. Biofouling in milli-labyrinth channels of drip irrigation systems using reclaimed wastewater: A review of optical methods and numerical modelling. *J. Environ. Manag.* **2026**, *397*, 128377. https://doi.org/10.1016/j.jenvman.2025.128377.
185. Sivakumar, A.D.; Sharma, R.; Wang, J.; et al. Dual-Channel Microfluidic Photoionization Detector. *Anal. Chem.* **2025**, *97*, 22397–22406. https://doi.org/10.1021/acs.analchem.5c05021.
186. Pfaller, M.A.; Andes, D.; Diekema, D.J.; et al. Wild-type MIC distributions, epidemiological cutoff values and species-specific clinical breakpoints for fluconazole and Candida: Time for harmonization of CLSI and EUCAST broth microdilution methods. *Drug Resist. Updates* **2010**, *13*, 180–195. https://doi.org/10.1016/j.drup.2010.09.002.
187. Zhang, K.; Khosravi, B.; Vahdati, S.; et al. FDA Review of Radiologic AI Algorithms: Process and Challenges. *Radiology* **2024**, *310*, e230242. https://doi.org/10.1148/radiol.230242.
188. Hay, S.I.; Rao, P.C.; Dolecek, C.; et al. Measuring and mapping the global burden of antimicrobial resistance. *BMC Med.* **2018**, *16*, 78. https://doi.org/10.1186/s12916-018-1073-z.
189. Fang, G.Y.; Mu, X.J.; Huang, B.W.; et al. Monitoring Longitudinal Trends and Assessment of the Health Risk of Shigella flexneri Antimicrobial Resistance. *Environ. Sci. Technol.* **2023**, *57*, 4971–4983. https://doi.org/10.1021/acs.est.2c08766.
190. Arnold, K.E.; Laing, G.; McMahon, B.J.; et al. The need for One Health systems-thinking approaches to understand multiscale dissemination of antimicrobial resistance. *Lancet Planet. Health* **2024**, *8*, e124–e133. https://doi.org/10.1016/s2542-5196(23)00278-4.
191. Zhou, H.; Guo, W.; Hao, T.; et al. Electrochemical sensor for single-cell determination of bacteria based on target-triggered click chemistry and fast scan voltammetry. *Food Chem.* **2023**, *417*, 135906. https://doi.org/10.1016/j.foodchem.2023.135906.

192. Chen, L.; Chen, F.; Liu, G.; et al. Superhydrophobic Functionalized $Ti_3C_2T_x$ MXene-Based Skin-Attachable and Wearable Electrochemical pH Sensor for Real-Time Sweat Detection. *Anal. Chem.* **2022**, *94*, 7319–7328. https://doi.org/10.1021/acs.analchem.2c00684.
193. Gao, W.; Xu, H.; Sun, X.; et al. An integrated wearable photo-electrochemical sensor for visible light amplified uric acid monitoring in sweat. *Biosens. Bioelectron.* **2025**, *289*, 117892. https://doi.org/10.1016/j.bios.2025.117892.